Synoptic- and Frontal-Scale Influences on Tropical Transition Events in the Atlantic Basin. Part II: Tropical Transition of Hurricane Karen

ANDREW L. HULME AND JONATHAN E. MARTIN

Department of Atmospheric and Oceanic Sciences, University of Wisconsin—Madison, Madison, Wisconsin

(Manuscript received 23 September 2008, in final form 27 May 2009)

ABSTRACT

A finescale simulation of the tropical transition of Atlantic Hurricane Karen in October 2001 is examined to determine the processes leading to the development of upshear convection and its effects on the process of tropical transition. The analysis shows that, as in marine extratropical cyclones, the area upshear of the pretransition cyclone is characterized by reduced stability. Lower-tropospheric frontogenesis leads to an intense burst of convection there and instigates three important processes that combine to produce a full-fledged tropical cyclone. First, the convection generates intense low-level vorticity on the western half of the cyclone, which quickly dominates the cyclone's vorticity field eventually organizing the circulation into a small-scale, intense vortex. Second, the diabatically enhanced circulation hastens the isolation of the cyclone's developing warm core by intensifying cold air advection on the northern and western sides of the storm and by placing evaporatively cooled air into the boundary layer to the south of the cyclone. Third, upshear convection vertically redistributes potential vorticity (PV) from the tropopause to the surface and introduces a component to the upper-level winds, which advects strong, shear-inducing PV gradients away from the column above the cyclone. These three processes transform the initial extratropical cyclone into a frontless vortex with tropical storm–force winds and a warm core in a low-shear environment. These features are sufficient, given a warm enough ocean surface, to allow self-amplification of the storm as a tropical cyclone.

The results further blur the distinction between tropical and extratropical cyclones as many of the processes identified as important to transition are similar to those that characterize ordinary marine cyclones and the extratropical occlusion process with the key distinctions being that here the convection is stronger and the initial upper-level feature is weaker. Thus, tropical transition of strong extratropical precursors follows the canonical midlatitude cyclone life cycle with upshear convection serving as the catalyst that both induces and organizes processes that favor tropical cyclogenesis in the postmature phase.

1. Introduction

In Hulme and Martin (2009, hereafter Part I) a survey of six recent examples of tropical transition of strong extratropical cyclones (SECs; Davis and Bosart 2004) was presented. For a review of recent literature relevant to this study, the reader is referred to section 1 of Part I. That analysis focused on the lower-tropospheric frontogenesis observed in the occluded quadrant of each storm just prior to transition. It was suggested that the ascending branch of the associated frontogenetic circulation generated low-level potential vorticity (PV) via latent heat release and that a positive feedback between the diabatically generated PV and subsequent frontogenesis resulted in an upshear convective burst that served as the proximate cause of the transition. In this paper, output from a finescale numerical simulation is employed in a detailed investigation of the role of upshear convection in the tropical transition of Atlantic Hurricane Karen (October 2001). Particular attention is paid to the interactions between frontogenesis, diabatic heating, and the evolution of the upper- and lower-tropospheric PV in transforming an initially vertically sheared, midlatitude, baroclinic disturbance into a vertically stacked, warm-core cyclone capable of nurturing a tropical storm.

The paper presents a synoptic overview of the cyclone that became Karen in section 2. Section 3 describes the numerical model employed in the study and offers a modest model evaluation through comparison of certain output parameters to observations. The analysis of the

Corresponding author address: Jonathan E. Martin, Department of Atmospheric and Oceanic Sciences, University of Wisconsin—Madison, 1225 W. Dayton St., Madison, WI 53705.
E-mail: jemarti1@wisc.edu

DOI: 10.1175/2009MWR2803.1

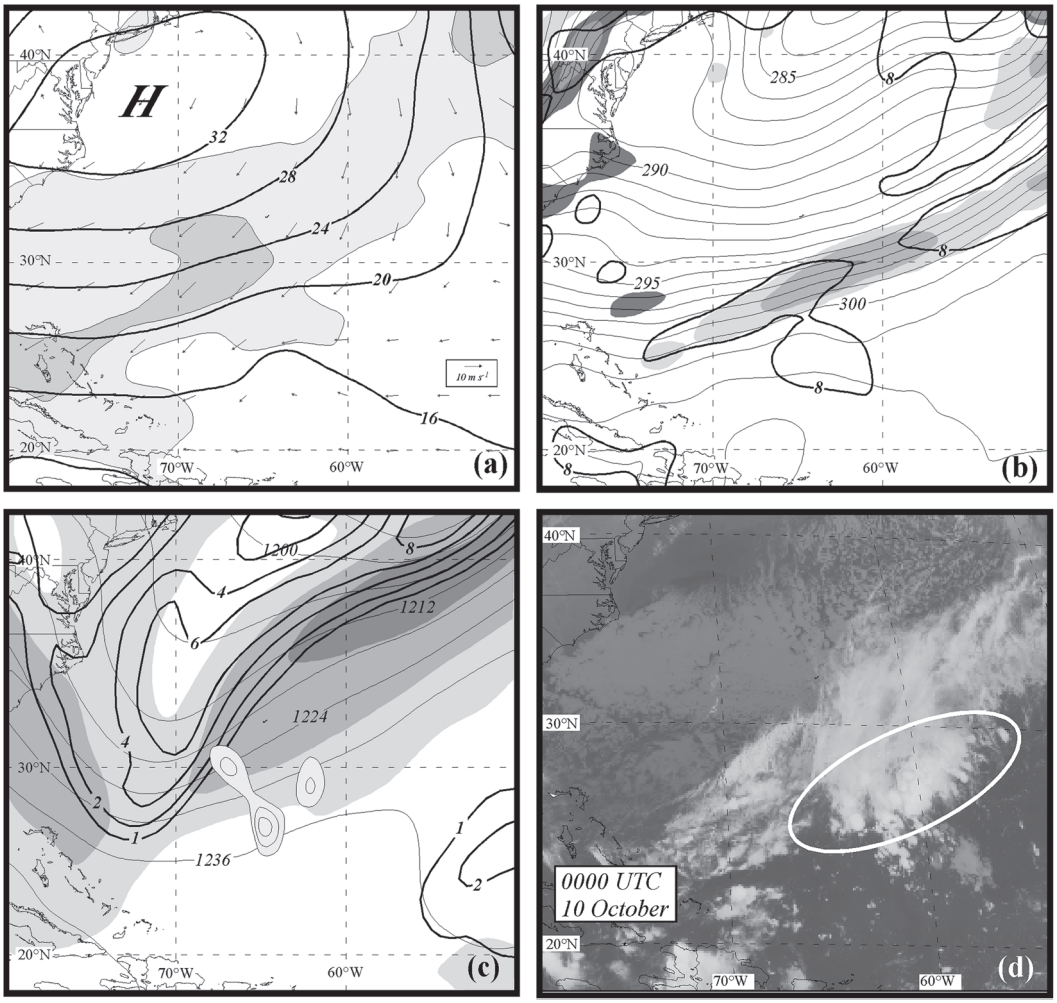

FIG. 1. (a) NCEP Global Forecast System FNL analyses of SLP (thick solid lines) and 900-hPa wind speed (shaded and arrows) at 0000 UTC 10 Oct 2001. SLP labeled in hPa and contoured every 4 hPa. Wind speed shaded every 5 m s^{-1} beginning at 10 m s^{-1}. "H" and "L" represents position of SLP maxima and minima. (b) FNL analyses of 900-hPa absolute vorticity (thick solid lines), 900-hPa potential temperature (thin solid lines), and 900-hPa frontogenesis (shaded) at 0000 UTC 10 Oct 2001. Vorticity labeled in 10^{-5} s^{-1} and contoured every 8×10^{-5} s^{-1} beginning at 8×10^{-5} s^{-1}. Potential temperature labeled in K and contoured every 1 K. Frontogenesis labeled in frontogenesis units [FGU; 1 FGU $\equiv$ K (100 km)$^{-1}$ (3 h)$^{-1}$] and shaded every 0.2 FGU with positive (negative) values in light (dark) shading. (c) FNL analyses of 200–250-hPa layer PV (thick lines), 200-hPa geopotential height (thin lines), 200-hPa wind speed (shaded), and regions of positive advection of 700-hPa geostrophic vorticity by the 500–900-hPa thermal wind (thin black lines with shading) at 0000 UTC 10 Oct 2001. PV labeled and contoured in PVU at 1, 2, 4, 6, and 8 PVU. Geopotential heights are labeled in dm and contoured every 6 dm. Wind speed is shaded every 20 m s^{-1} beginning at 15 m s^{-1}. PVA is labeled in 10^{-9} m kg^{-1} and contoured every 2×10^{-9} m kg^{-1} starting at 2×10^{-9} m kg^{-1}. (d) Infrared satellite image from 2315 UTC 9 Oct 2001. The oval highlights a region mentioned in the text.

model output is presented in section 4, while a summary and conclusions are offered in section 5.

2. Synoptic overview

The synoptic elements important to the cyclogenesis of Karen began to interact over the subtropical Atlantic Ocean on 9 October 2001 (hereafter, all dates are in 2001) when a cyclone progressed quickly across the North Atlantic at 45°N latitude and dragged a cold front into the subtropics just south of Bermuda. On 10 October, an inverted sea level pressure (SLP) trough began to develop around 25°N, 65°W on the warm side of this front (Fig. 1a). Concurrently, a zonally oriented strip of low-level vorticity became isolated from the front just to the south of an active area of frontogenesis (Fig. 1b). To the

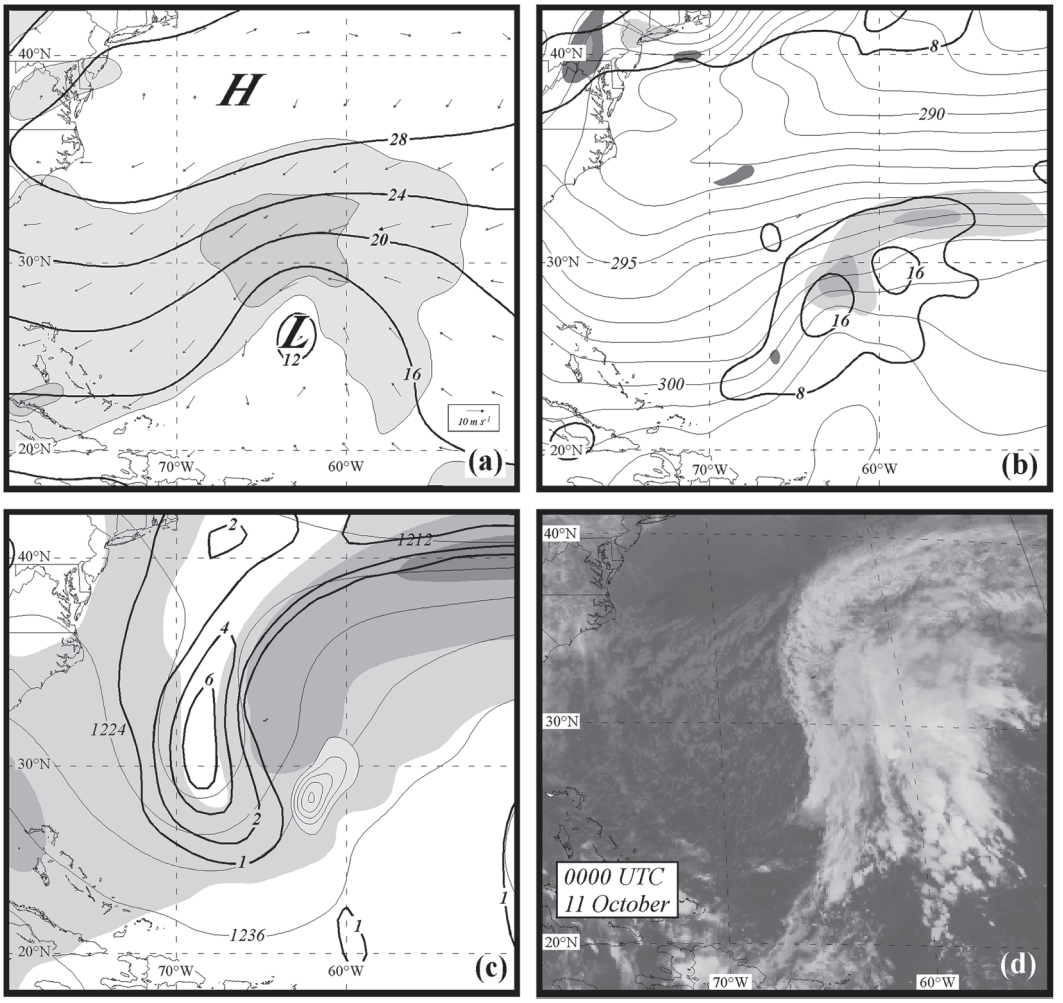

FIG. 2. As in Fig. 1, but for (a) 0000 UTC 11 Oct 2001, (b) 0000 UTC 11 Oct 2001, and (c) 0000 UTC 11 Oct 2001. (d) Infrared satellite image from 2315 UTC 10 Oct 2001.

west of these surface features, an upper-level trough developed and amplified off the coast at ~70°W (Fig. 1c). The frontogenesis along the front was manifest in the southwest–northeast-oriented line of disturbed weather apparent in the satellite imagery (Fig. 1d).

By 0000 UTC 11 October, the inverted trough had developed into a closed SLP minimum at the peak of a thermal ridge (Figs. 2a,b). To the north of the cyclone, frontogenesis was occurring along the cyclone's warm front in association with strong confluence in easterly flow. At upper levels, the trough had moved southeastward and the upper-level PV feature became more compact (Fig. 2c). In this alignment, Karen's precursor (hereafter, Karen refers to the surface cyclone at any stage) was placed immediately downshear of a potent upper-tropospheric PV maximum. Ridging downstream of the cyclone/trough, apparent in the 200-hPa height and upper-level PV fields as well as in the satellite cloud canopy (Fig. 2d), suggests that condensational heating from the system was already beginning to feedback onto the large-scale flow.

In the subsequent 12 h, Karen began heading to the northwest and was located approximately 200 km from Bermuda by 0000 UTC 12 October (Fig. 3a). By this time, the low-level winds in the northwest quadrant of the storm had increased to around 30 m s^{-1}. At the surface, near-hurricane-strength winds, 30 m s^{-1} sustained winds with gusts to 40 m s^{-1}, were observed at St. George, Bermuda (BDA; Beven et al. 2003). The northwest quadrant was also an area of particularly intense frontogenesis along the cyclone's now bent-back warm front (Fig. 3b). On the western flank of the front, cooler air began to wrap around the southern half of the cyclone. As Karen progressed northwestward, the upper-level trough was drastically weakened and the PV anomaly began to acquire the treble clef structure

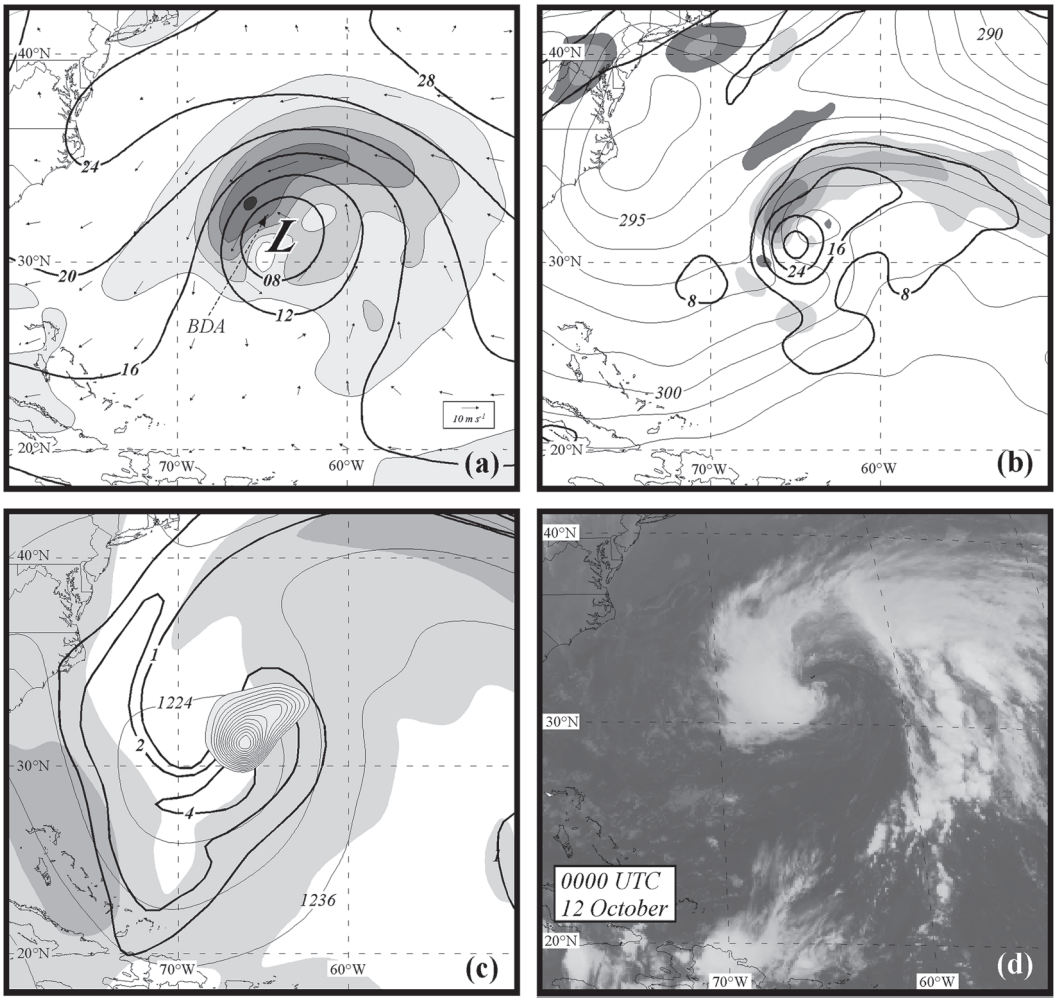

FIG. 3. As in Fig. 1, but for (a) 0000 UTC 12 Oct 2001, (b) 0000 UTC 12 Oct 2001, and (c) 0000 UTC 12 Oct 2001. (d) Infrared satellite image from 2315 UTC 11 Oct 2001.

(Fig. 3c) characteristic of occluded cyclones (Martin 1998). Also consistent with the commencement of occlusion was the fact that Karen had, by this time, moved onto the cold side of the upper-level jet and moved away from the peak of the thermal ridge. The satellite image from this time reveals intense thunderstorms to the north and west of the cyclone center. In light of these changes, Karen was given a subtropical designation by the National Hurricane Center (NHC) at this time.

After 0000 UTC 12 October, Karen began to quickly lose its frontal structure and acquire tropical characteristics. The near-surface wind field, which was initially characterized by strong winds on only the northern semicircle of the cyclone, became axisymmetric with a ring of wind speeds greater than 15 m s^{-1} surrounding the cyclone center (Fig. 4a). Frontogenesis in the vicinity of the cyclone also decreased in magnitude as temperature gradients around the SLP minimum weakened (Fig. 4b). While the frontal zones collapsed, a warm core began to develop at the center of the cyclone (Fig. 4b) and would eventually occupy the entire tropospheric column by 0000 UTC 13 October (not shown). By 0000 UTC 13 October the upper-level PV field was weakened further as the isolation of the PV anomaly from the midlatitudes became complete (Fig. 4c). Additionally, Karen had moved under the axis of the upper-level PV maximum (and elongated upper-level shortwave trough axis). Consequently, the vertical shear, which had been in excess of 15 m s^{-1} at 0000 UTC 12 October, had decreased to well below that threshold[1] by this time (Table 1). In satellite imagery, the deep convection to

[1] Generally, unless the vertical shear in the 200–900-hPa layer is less than 10–15 m s^{-1}, tropical cyclogenesis is unlikely (e.g., DeMaria et al. 2001).

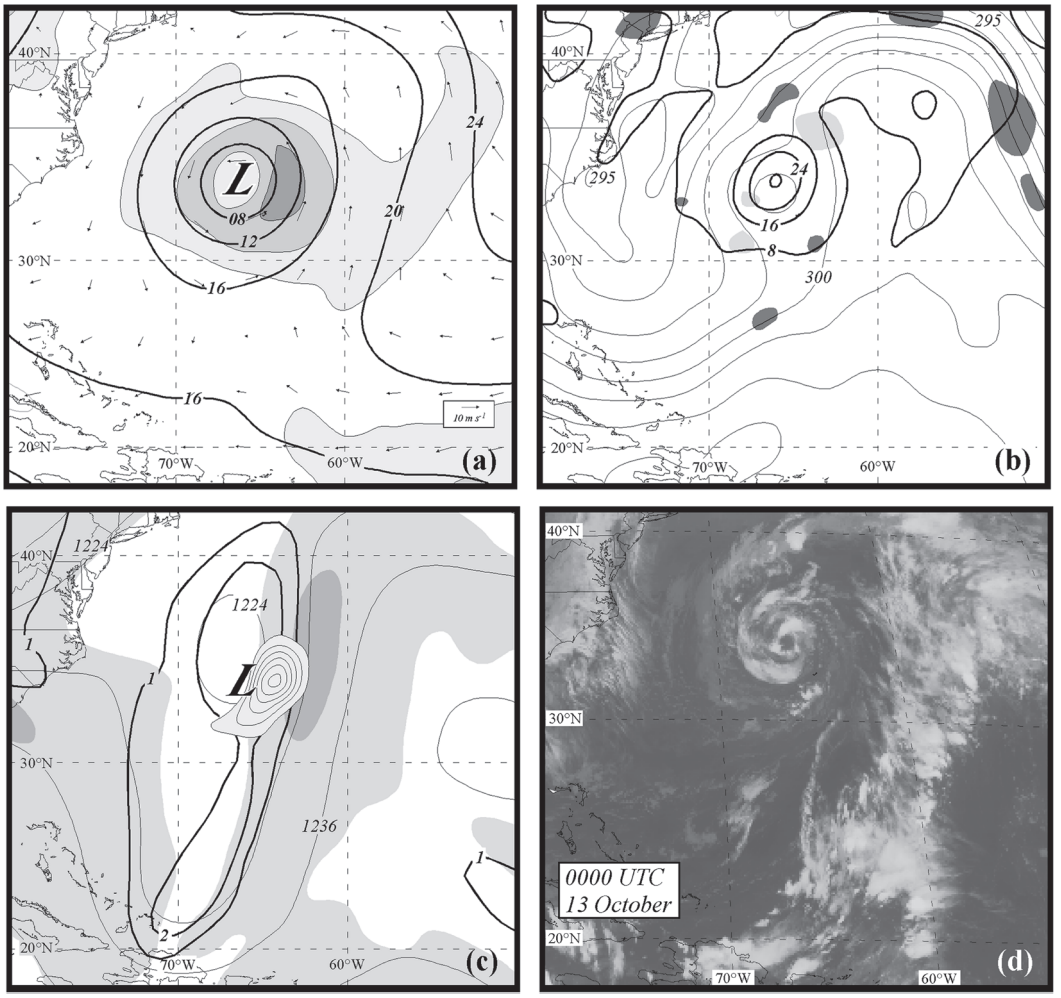

FIG. 4. As in Fig. 1, but for (a) 0000 UTC 13 Oct 2001, (b) 0000 UTC 13 Oct 2001, and (c) 0000 UTC 13 Oct 2001. (d) Infrared satellite image from 2315 UTC 12 Oct 2001.

the northwest of the cyclone that began on 11 October had collapsed (Fig. 4d). In its wake, a small eyelike feature developed around 1200 UTC 12 October and was still evident at 0000 UTC 13 October. Repeated convective bursts occurred around this nascent eye over the next 24 h. With weak vertical shear over the vortex, Karen was able to maintain tropical characteristics and was designated tropical by the Hurricane Best Track (HURDAT) database compiled by the Tropical Prediction Center (TPC) at 0600 UTC 13 October.[2] The tropical cyclone continued to move northward, briefly reaching hurricane strength on 14 October before making landfall in Nova Scotia on 15 October as a weak extratropical-transitioning tropical storm (e.g., Jones et al. 2003).

3. Model description and evaluation

To better understand the physical factors involved in this case of tropical transition, we employ a numerical simulation of Karen run utilizing version 2 of the Weather Research and Forecasting (WRF) modeling system with the Advanced Research WRF (ARW) solver as described by Skamarock et al. (2005). The WRF model integrates the fully compressible, Euler nonhydrostatic equations while conserving scalar variables. Specific physical parameterizations employed in the simulation include the WRF Single-Moment 6-Class (WSM6) cloud microphysics package (Hong and Lim 2006), the modified version of the Kain–Fritsch formulation (KF2; Kain and Fritsch 1990, 1993), and the Yonsei University (YSU)

[2] The cyclone phase space diagnostics of Hart (2003) suggests Karen became tropical earlier, ~1200 UTC 12 October, when the storm first became "warm core/symmetric."

TABLE 1. Magnitude of the 200–900-hPa vertical shear (m s^{-1}) over the cyclone center at 3-h intervals calculated from the WRF model (domain 1) output. The cyclone center was defined as a local maximum of 900-hPa relative vorticity averaged over a 5 by 5 square on grid 1 (135 km × 135 km). The shear was averaged over an 81 km × 81 km box.

Time	200–900-hPa shear (m s^{-1})
0000 UTC 11 Oct	25
0300 UTC 11 Oct	26
0600 UTC 11 Oct	30
0900 UTC 11 Oct	30.5
1200 UTC 11 Oct	31
1500 UTC 11 Oct	26.5
1800 UTC 11 Oct	25
2100 UTC 11 Oct	26
0000 UTC 12 Oct	17
0300 UTC 12 Oct	16
0600 UTC 12 Oct	14
0900 UTC 12 Oct	12
1200 UTC 12 Oct	10
1500 UTC 12 Oct	9
1800 UTC 12 Oct	8
2100 UTC 12 Oct	7
0000 UTC 13 Oct	8.5

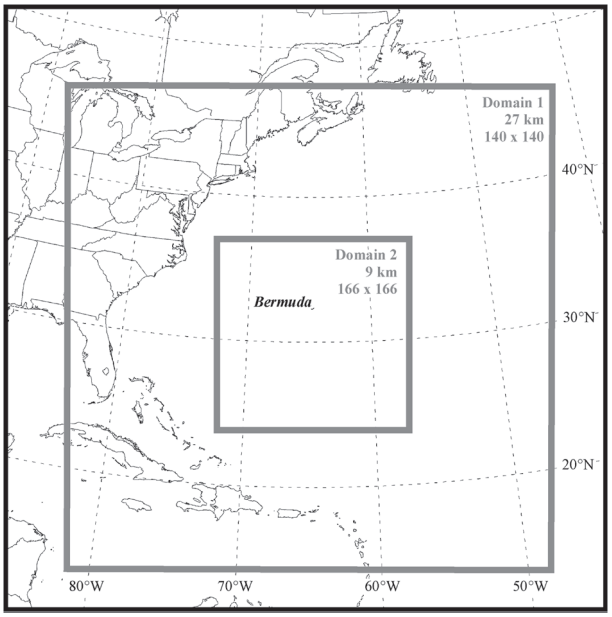

FIG. 5. Domains for the nested WRF simulation described in the text.

planetary boundary layer (PBL) parameterization (Hong et al. 2006). Radiative transfer is simulated using a combination of the Rapid Radiative Transfer Model (RRTM; Mlawer et al. 1997) for longwave radiation and the Dudhia (1989) shortwave radiation scheme.

The simulation is initialized with data obtained from the National Centers for Environmental Prediction (NCEP) Global Forecast System final analysis (FNL) dataset with a 1° × 1° grid spacing. The outermost lateral boundary conditions derived from that dataset are linearly interpolated between each 6-hourly global analysis time. Vertical interpolation is onto 31 terrain-following full-η layers with highest vertical resolution near the surface and a model top at 50 hPa. The model domain, shown in Fig. 5, consists of two nested grids: a coarser outer domain with a grid spacing of 27 km and a time step of 80 s, and a fine inner domain with a grid spacing of 9 km and a time step of 26.67 s. The simulation employs a two-way nesting scheme in which information is traded in both directions between the outer and inner domains. The simulation of Karen lasts 48 h and is initialized at 0000 UTC 11 October 2001. Model output was interpolated onto 41 isobaric levels at 25-hPa intervals between 1000 and 100 hPa. Additional data like 10-m winds, 2-m temperature, and specific humidity were also interpolated to provide near-surface data.

Since much of the ensuing analysis relies on an accurate portrayal of features only resolvable through a mesoscale model, a short evaluation of the simulation is presented with particular attention given to the model's depiction of convection. Figure 6 compares the location and strength of the SLP minimum from the simulation of Karen with the observed data from HURDAT. The simulation accurately captures the general movement of Karen as the largest track error is approximately 110 km and occurs while Karen was an extratropical cyclone with a broad center approaching Bermuda. This error decreases once the center of Karen becomes better defined. The simulation strengthens the low at a slightly faster rate than observed for the first 30 h, deepening the SLP minimum to 984 hPa, 4 hPa deeper than what was observed, by 0600 UTC 12 October. After this time, the simulated storm weakens slowly to within 1 hPa of the observed SLP minimum by the end of the model run (0000 UTC 13 October). Slight weakening after the period of baroclinic strengthening and before the instigation of self-amplification by air–sea interaction has been observed in other studies of tropical transition (e.g., Davis and Bosart 2001, 2003) and appears to have characterized Karen. This tendency is reasonably well represented by the simulation.

Comparing hourly precipitation fields from the WRF simulation to satellite data [the Geostationary Operational Environmental Satellite Infrared (GOES-IR) and Special Sensor Microwave Imager (SSM/I) rain-rate data portrayed in Fig. 7 were obtained from the Naval Research Laboratory at Monterey, California, see online at www.nrlmry.navy.mil/tc_pages/tc_home.html] provides additional confidence in the model. For the first 24 h, the model correctly simulates the wrapping

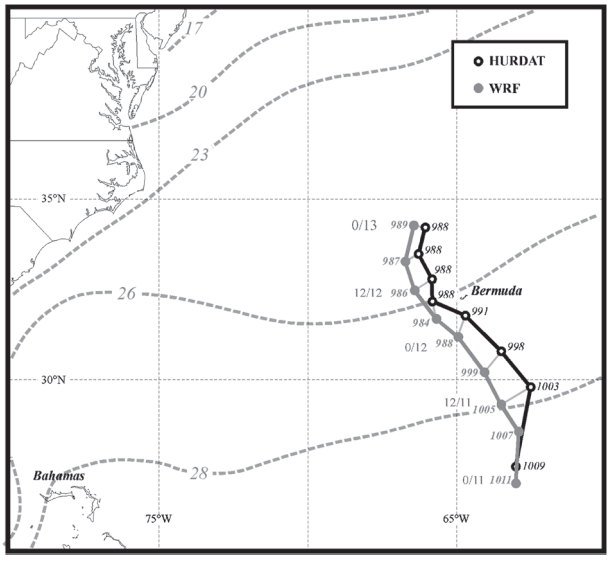

FIG. 6. Position of the SLP minimum at 6-h intervals from 0600 UTC 11 Oct 2001 to 0000 UTC 13 Oct 2001 according to the HURDAT database (open circles) and from 0000 UTC 11 Oct 2001 to 0000 UTC 13 Oct 2001 according to the WRF forecast (filled dots). Values of minimum sea level pressure are placed by the appropriate dot along with the time of the observation using the notation time/date. Thick dashed lines are isotherms of sea surface temperature labeled in °C and contoured at 28°, 26°, 23°, 20°, and 17°C obtained from the NCEP Realtime Global Sea Surface Temperature analysis (RTG-SST; available online at http://polar.ncep.noaa.gov/sst).

of precipitation around the center of Karen. This relationship is especially evident at about 2200 UTC 11 October (Figs. 7a,b) when a large area of convection was present to the west and northwest (upshear) of Karen in both the WRF run and in satellite imagery/retrieval. Additionally, the model correctly produces the eyelike feature toward the end of the simulation (Figs. 7c,d). The simulated near-surface wind field also agreed well with observations predicting a large of area of 30 m s^{-1} surface winds to the north of the cyclone at 0000 UTC 12 October, consistent with several reports of strong winds on Bermuda around that time as well as Quick Scatterometer (QuikSCAT) data reported in Bancroft (2002) (not shown). Since the model simulation of Karen's strength, track, and convective morphology is reasonably close to that of the actual storm, we believe the model run accurately captures the tropical transition of Karen and confidently employ the output in our subsequent diagnosis of this event.

4. Analysis

The analysis of the tropical transition of Karen focuses on four major elements: 1) the evolution of convection near the storm center, 2) the evolution of the low-level vorticity field, 3) the role of frontal processes in shaping 1) and 2), and 4) the effect of diabatic heating in transforming the PV field at upper- and lower-tropospheric levels. We begin by considering the evolution of convection.

a. Evolution of convection

During the course of the simulated 48 h, the convection around the center of Karen changed drastically. Figure 8 portrays the evolution of convection, using hourly rainfall rates, and 10-m winds from the inner-domain at 6-h intervals. Early in the simulation (0900 UTC 11 October), rainfall was almost entirely confined to two bands: a cold-frontal band extending to the east and the south (not shown), and a warm-frontal band extending to the east-northeast (Fig. 8a). The most intense convection occurred at the western end of the warm front just to the north of the SLP minimum. At this time, the center of Karen was relatively poorly organized and asymmetric with strongest winds to the northwest of the cyclone's SLP minimum along the warm front (Fig. 8b).

At 1500 UTC, a strong pulse of convection developed at the western end of the warm front which had extended back behind the SLP minimum on the upshear side of the cyclone (Fig. 8c). Northeasterly near-surface wind speeds increased to over 25 m s^{-1} in the cyclone's western half by this time (Fig. 8d). Over the next 6 h, the convective burst increased in intensity and areal coverage so that, by 2100 UTC 11 October, the most intense precipitation was directly to the west of the SLP minimum (Fig. 8e), which had progressed persistently westward following the isallobaric tendencies induced by the intense local convection (not shown). At this time, a region of tropical storm–force (30 m s^{-1}) westerly winds developed, extending from the southern edge of the strongest convection to south of the cyclone center (Fig. 8f). The center of Karen continued to progress to the northwest as the weakening upshear convection became centered to the south of the SLP minimum by 0300 UTC 12 October (Fig. 8g). However, by this time, Karen had developed a tight, axisymmetric structure with 30 m s^{-1} near-surface winds nearly ringing a vortex of 90-km radius (Fig. 8h). During the 12-h period of intense upshear convection, ending at 0300 UTC 12 October, Karen's minimum SLP dropped from 1002 to 985 hPa.

After 0300 UTC 12 October, the convection collapsed and Karen's progression to the west was halted. By 0900 UTC 12 October, relatively weak convection occurred ~100 km to the north of the SLP minimum in what appeared to be the building of an eyewall (Fig. 8i)

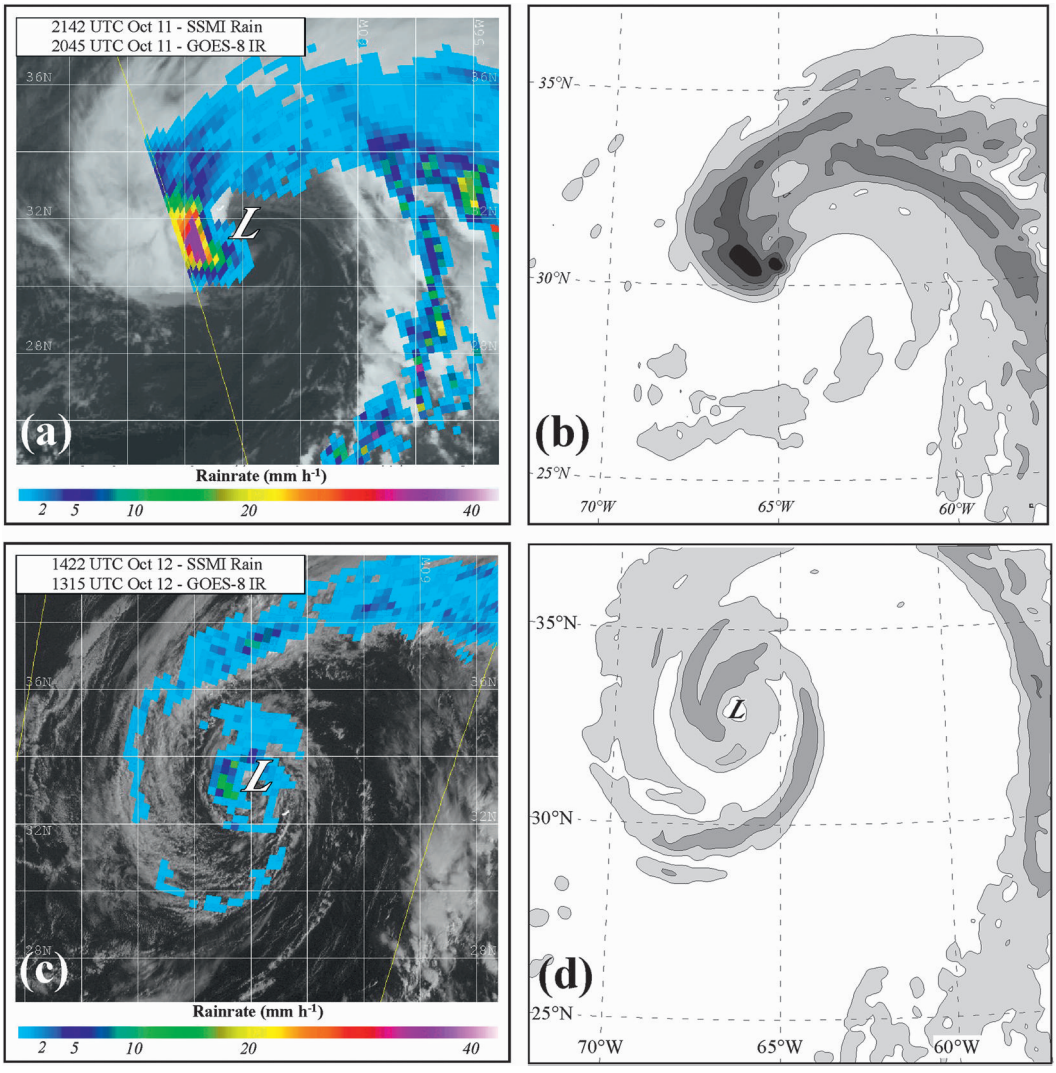

FIG. 7. (a) Satellite mosaic of *GOES-8* infrared and SSM/I rain-rate product from the Naval Research Laboratory (NRL, available online at http://www.nrlmry.navy.mil/tc_pages/tc_home.html) from 2045 UTC 11 Oct 2001 and 2142 UTC 11 Oct 2001, respectively. Rain rate in mm h^{-1} indicated by the color bar. (b) WRF forecast of hourly rain rate valid at 2200 UTC 11 Oct 2001. Rain rate is shaded in units of mm h^{-1} at increments of 0.25, 2, 5, 10, 20, and 40 mm h^{-1}. (c) Satellite mosaic of *GOES-8* infrared and SSM/I rain-rate products from 1315 UTC 12 Oct 2001 and 1422 UTC 12 Oct 2001, respectively. (d) As in (b), but valid at 1400 UTC 12 Oct 2001. Note that the map projection and display area differ between the satellite and WRF images. The "L" in (a) and (c) represent the position of the SLP minimum.

while wind speeds on the western half of the vortex decreased (Fig. 8j). Six hours later, precipitation around the cyclone continued to weaken (Fig. 8k). Although near-surface winds speeds slightly decreased by 1500 UTC 12 October, the wind field around the vortex became more uniform and axisymmetric (Fig. 8l).

During Karen's progression toward transition, the surface cyclone center appeared to be drawn toward the convection resulting in a westward translation of the SLP minimum during the period of most intense upshear convection. This behavior is consistent with diabatic production of low-level PV associated with deep convective heating and its associated height falls. Additionally, the transition of Karen exhibited a characteristic sequence of intense convection, followed by intensification of the vortex and subsequent reorganization into a tropical cyclone that has been observed in other cases of moderately sheared tropical cyclogenesis such as Hurricane Diana (1984) (Davis and Bosart 2001) and Hurricane Danny (1997) (Molinari et al. 2004). Both of these cases are in the WEC category suggested by Davis and Bosart (2004) while Karen is in the SEC category.

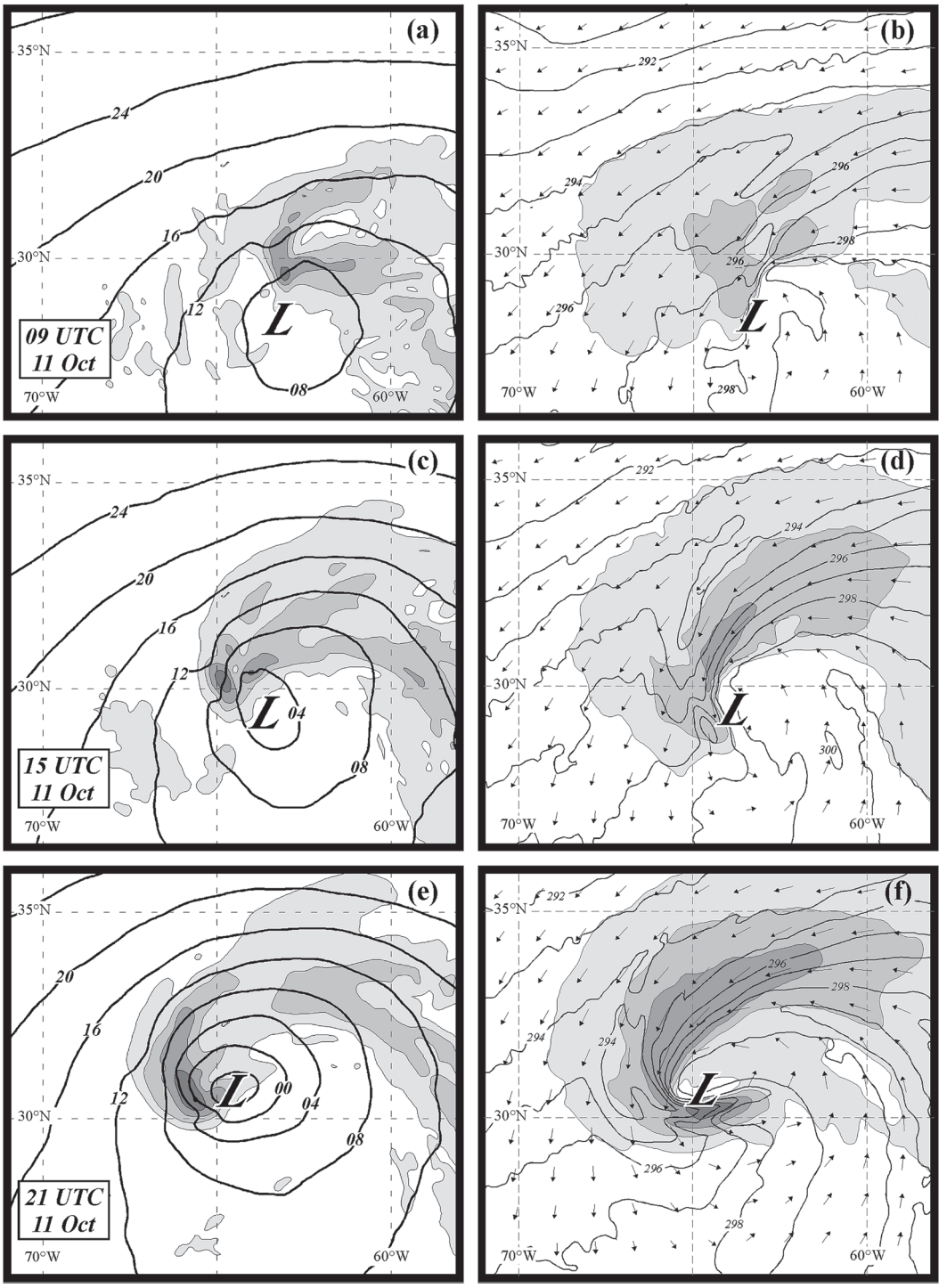

FIG. 8. (a) WRF forecast of sea level pressure (thick lines, labeled and contoured as in Fig. 1a) and hourly rain rate (shaded as in Fig. 7b) valid at 0900 UTC 11 Oct 2001. (b) WRF forecast of 10-m winds and 950-hPa potential temperature (black lines) valid at 0900 UTC 11 Oct 2001. Arrows represent the wind vector and speeds are shaded at increments of 5 m s^{-1} beginning at 15 m s^{-1}. Potential temperature is labeled in K and contoured every 1 K. (c) As in (a), but for 1500 UTC 11 Oct 2001. (d) As in (b), but for 1500 UTC 11 Oct 2001. (e) As in (a), but for 2100 UTC 11 Oct 2001. (f) As in (b), but for 2100 UTC 11 Oct 2001. (g) As in (a), but for 0300 UTC 12 Oct 2001. (h) As in (b), but for 0300 UTC 12 Oct 2001. (i) As in (a), but for 0900 UTC 12 Oct 2001. (j) As in (b), but for 0900 UTC 12 Oct 2001. (k) As in (a), but for 1500 UTC 12 Oct 2001. (l) As in (b), but for 1500 UTC 12 Oct 2001. The ''L'' in (a)–(l) represents the position of the SLP minimum.

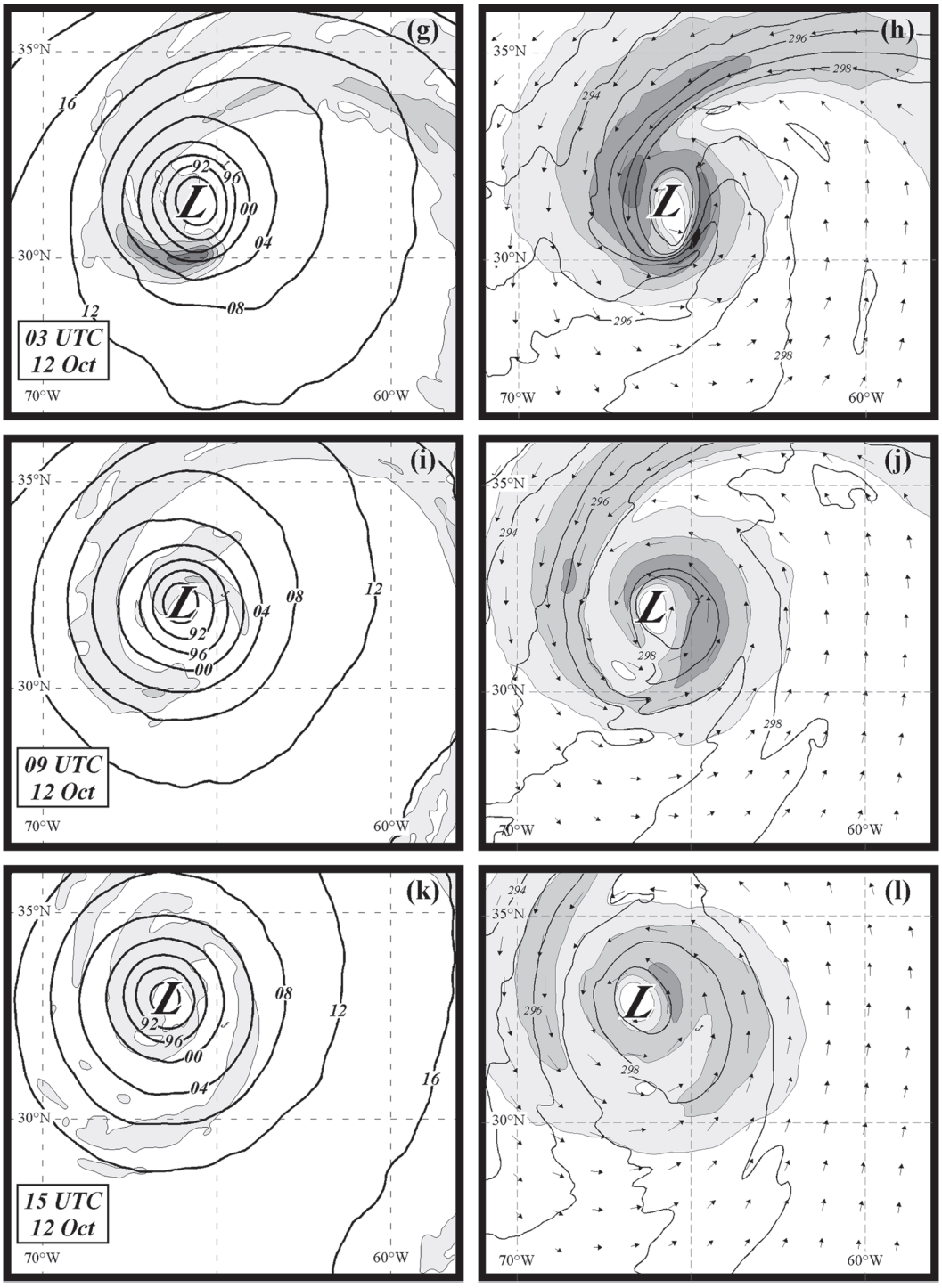

FIG. 8. (*Continued*)

As subsequent analysis will show, the organization of the important transition-inducing convection in this particular SEC depends upon the frontal structure and frontal dynamics of the extratropical precursor.

b. Low-level vorticity

The evolution of Karen's low-level vorticity field offers an alternative perspective on the process of transition.

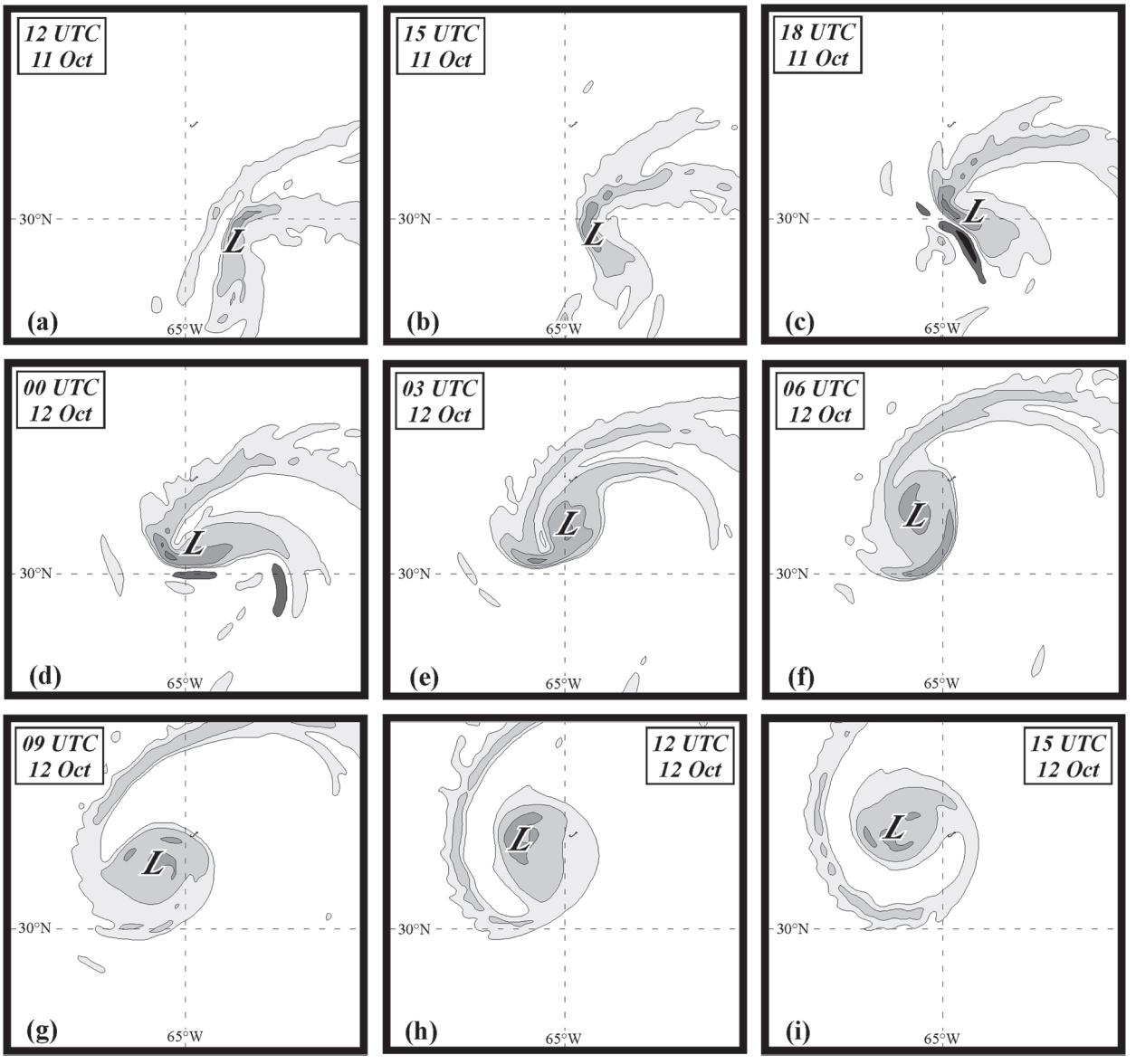

FIG. 9. WRF forecast of 900-hPa absolute vorticity valid at (a) 1200 UTC 11 Oct 2001, (b) 1500 UTC 11 Oct 2001, (c) 1800 UTC 11 Oct 2001, (d) 0000 UTC 12 Oct 2001, (e) 0300 UTC 12 Oct 2001, (f) 0600 UTC 12 Oct 2001, (g) 0900 UTC 12 Oct 2001, (h) 1200 UTC 12 Oct 2001, and (i) 1500 UTC 12 Oct 2001. Vorticity is in units of 10^{-4} s^{-1} with positive (negative) values lightly (darkly) shaded at increments of 2, 4, 8, and 16×10^{-4} s^{-1} (-2, -4, -8, and -16×10^{-4} s^{-1}). The "L" in (a)–(i) represents the position of the SLP minimum.

Figure 9 portrays the evolution of the simulated 900-hPa absolute vorticity during the transition of Karen into a tropical cyclone. While the storm was still frontal in nature, vorticity increases in the northwest quadrant of the cyclone were coincident with the convection that formed along the bent-back warm front (cf. Figs. 9a,b). At 1500 UTC 11 October, a strip of vorticity stretched from near the SLP minimum northeastward along the system's warm front (Fig. 9b). Circular pockets of enhanced vorticity superimposed on this strip were associated with distinct areas of intense convection (see Fig. 8c). By 1800 UTC 11 October, the largest vorticity was directly west of the cyclone center, collocated with the upshear convective outburst discussed earlier, and was beginning to cyclonically wrap around the cyclone center (Fig. 9c). Coincident with the development of the vorticity maximum, a companion area of negative vorticity developed to its south and west. This shear vorticity couplet accompanied an intense northwesterly wind maximum that developed at this time. By

0000 UTC 12 October, most of the absolute vorticity had become associated with the center of the cyclone and had begun to adopt an elliptical distribution (Fig. 9d). The linear band on the southwestern flank began to diminish at 0300 UTC 12 October as vorticity continued to sweep around to the center of the cyclone (Fig. 9e) By 0600 UTC 12 October, the linear band had nearly disappeared and almost all remaining vorticity had become centered on the SLP minimum (Fig. 9f). At this time, the simulated cyclone reached its minimum sea level pressure. For the last 18 h of the simulation, the absolute vorticity remained circular and centered on the SLP minimum with a weak, vestigial frontal band spiraling out from the center (Figs. 9g,h,i).

The sudden increase in the western, linear vorticity maximum (Fig. 9c) and the appearance of negative vorticity between 1500 and 1800 UTC 11 October were coincident with the strong burst of convection on the upshear side of the cyclone and with the start of the period in which the vorticity field began a shift in orientation from frontal and linear to circular and axisymmetric. Thus, it appears that the upshear convective burst altered the method by which low-level vorticity was both created and distributed in the cyclone environment. To test this hypothesis, vorticity tendency terms were calculated using the isobaric vorticity tendency equation:

$$\frac{\partial \eta_p}{\partial t} = -\mathbf{v} \cdot \nabla \eta_p - \omega \frac{\partial \eta_p}{\partial p} - \eta_p (\nabla \cdot \mathbf{v}) + \mathbf{k} \cdot \left(\frac{\partial \mathbf{v}}{\partial p} \times \nabla \omega \right), \quad (1)$$

where η_p is the vertical component of absolute vorticity on an isobaric surface, $\mathbf{v}$ is the horizontal wind vector, ω is the vertical motion, and ∇ is the horizontal gradient operator. The right-hand-side (RHS) terms of (1) are typically referred to as the horizontal advection, vertical advection, stretching, and tilting terms, respectively.

During the initial phase of the transition process, represented by conditions at 1200 UTC 11 October, low-level vorticity generation by the stretching term occurred mostly to the north and east of the cyclone center along the warm/bent-back front (Fig. 10a). Since the winds were nearly parallel to the front, horizontal vorticity advection at this time was directed down the warm front toward its western terminus (Fig. 10b). The sum of the tilting and vertical advection terms was much smaller than the stretching and horizontal advection terms at this time (not shown).

As the strong burst of upshear convection commenced at 1500 UTC, three distinct maxima of generation by stretching occurred along the front (Fig. 10c) each with an advection maximum occurring downwind along the front (Fig. 10d). Tilting and vertical advection were larger in magnitude at this time but were still dwarfed by the combination of stretching and horizontal advection (not shown).

By 1900 UTC, a single stretching maximum associated with the upshear convection was occurring at the end of the warm front to the west and northwest of the SLP minimum (Fig. 10e). At this time, however, negative advection occurred along nearly the entire length of the frontal vorticity strip (Fig. 10f) suggesting that the recently developed northwesterly low-level jet (LLJ) contained a significant cross-frontal wind component. At the longitude of the SLP minimum, a couplet of advection with positive values on the north side of the frontal vorticity band was evident. In this area, there was no vorticity generation by stretching or tilting implying that the increase in cyclonic vorticity around the SLP minimum at 1900 UTC resulted from advection and not from some in situ vorticity-generating process. Tilting and vertical advection remained relatively insignificant contributors to the overall vorticity tendency at 900 hPa at this time (not shown).

By 2200 UTC, the center of strongest vorticity generation via stretching had encroached upon the SLP minimum and mostly negative advection occurred along what had been the bent-back front (Figs. 10g,h). Positive advection to the northeast of the SLP minimum continued such that by 0300 UTC 12 October a circular area of vorticity was associated with the cyclone center (see Fig. 9e). In summary, when the vorticity field was mostly linear, vorticity was generated by stretching within the frontal zone and then advected southwestward to the western end of the bent-back warm front. With the burst of upshear convection and the coincident development of a strong LLJ directed partly across that front, a couplet of vorticity advection developed—negative (positive) south (north) of the frontal vorticity strip. This advection pattern promoted the amalgamation of vorticity near the cyclone center. Thus, the intense burst of convection upshear of the surface cyclone and the coincident near-surface wind maximum appear to have altered the environment so as to transfer vorticity, produced in linear frontal bands, into a more isotropic pattern around the reorganizing center.

c. *Fronts and frontogenesis*

Part I showed that intense near-surface frontogenesis along a bent-back front coincident with upshear convection is characteristically antecedent to the tropical transition of SECs. In the simulation of Karen, the strongest frontogenesis initially occurred to the north

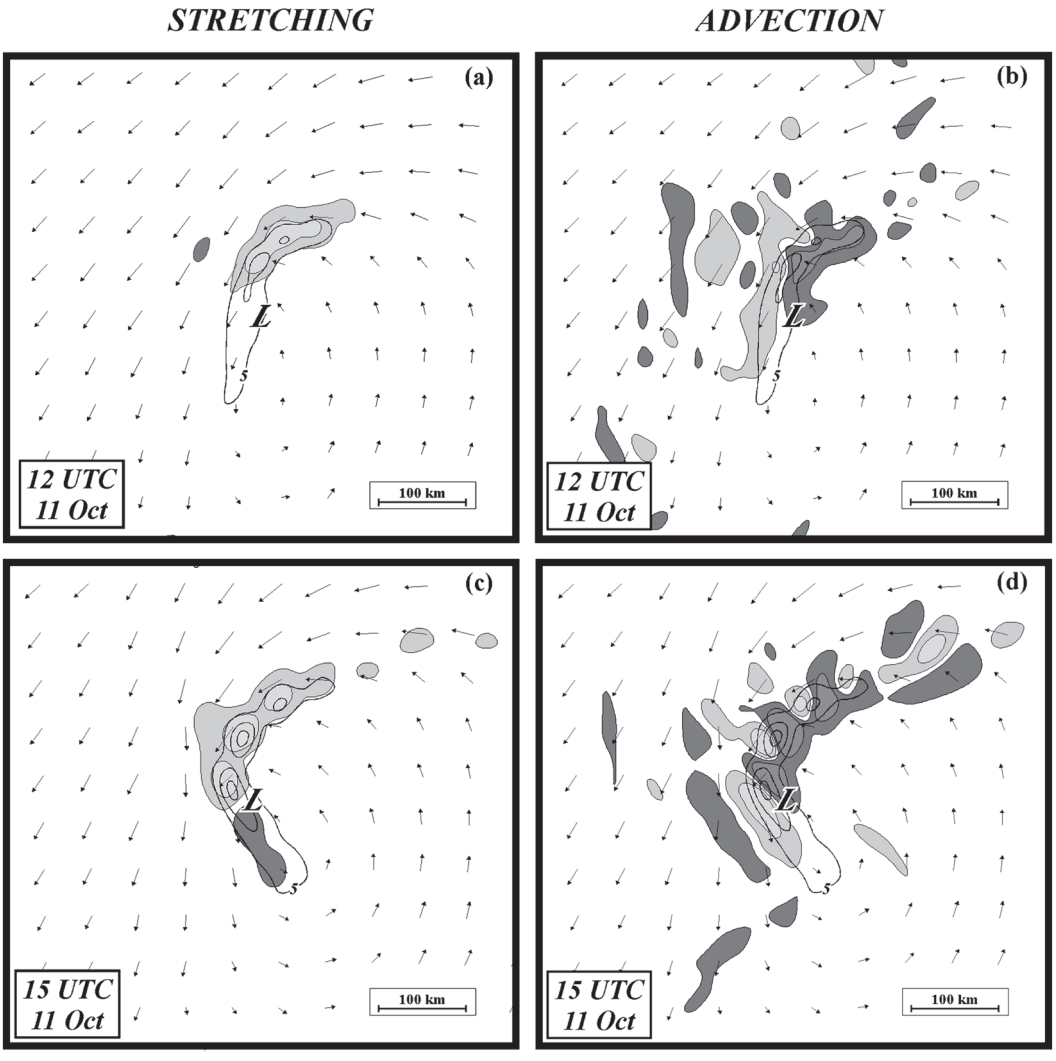

FIG. 10. (a) Absolute vorticity tendency at 900 hPa due to the stretching term (shaded), 900-hPa absolute vorticity (thick black lines), and 900-hPa winds (arrows) from the WRF forecast valid at 1200 UTC 11 Oct 2001. The stretching term is in units of 10^{-4} s^{-1} h^{-1} with positive (negative) values lightly (darkly) shaded at increments of 2, 8, and 32 $\times$ 10^{-4} s^{-1} h^{-1} (-2, -8, and -32×10^{-4} s^{-1} h^{-1}). Absolute vorticity in units of 10^{-4} s^{-1} contoured every 5 $\times$ 10^{-4} s^{-1} beginning at 5 $\times$ 10^{-4} s^{-1}. The "L" represents the position of the SLP minimum. (b) Absolute vorticity tendency at 900 hPa due to horizontal advection (shaded) and 900-hPa absolute vorticity (thick black lines) from the WRF forecast valid at 1200 UTC 11 Oct 2001. Horizontal advective tendency contoured and shaded as for stretching term in (a). Absolute vorticity labeled and contoured as in (a). (c) As in (a), but from the WRF forecast valid at 1500 UTC 11 Oct. (d) As in (b), but from the WRF forecast valid at 1500 UTC 11 Oct. (e) As in (a), but for the WRF forecast valid at 1900 UTC 11 Oct 2001. (f) As in (b), but for the WRF forecast valid at 1900 UTC 11 Oct 2001. (g) As in (a), but for the WRF forecast valid at 2200 UTC 11 Oct 2001. (h) As in (b), but for the WRF forecast valid at 2200 UTC 11 Oct 2001.

and northeast of the surface cyclone along the warm front (Fig. 11a). The associated thermally direct circulation produced ascent/latent heat release (LHR) on the warm side of the boundary which, in turn, generated low-level PV. With the commencement of the upshear convection at 1500 UTC 11 October, a couplet of positive and negative frontogenesis, of similar magnitudes, developed directly to the west of the cyclone (Fig. 11b). Intense downward vertical motion occurred in the middle of this couplet (not shown) as the thermally direct subsidence was stronger than the thermally indirect ascent to the west. Coincident with the area of descent, a cold tongue, stretching northwest to southeast, was present to the west of the cyclone center presumably induced by evaporative cooling. By 1800 UTC 11 October, temperature gradients sharpened substantially

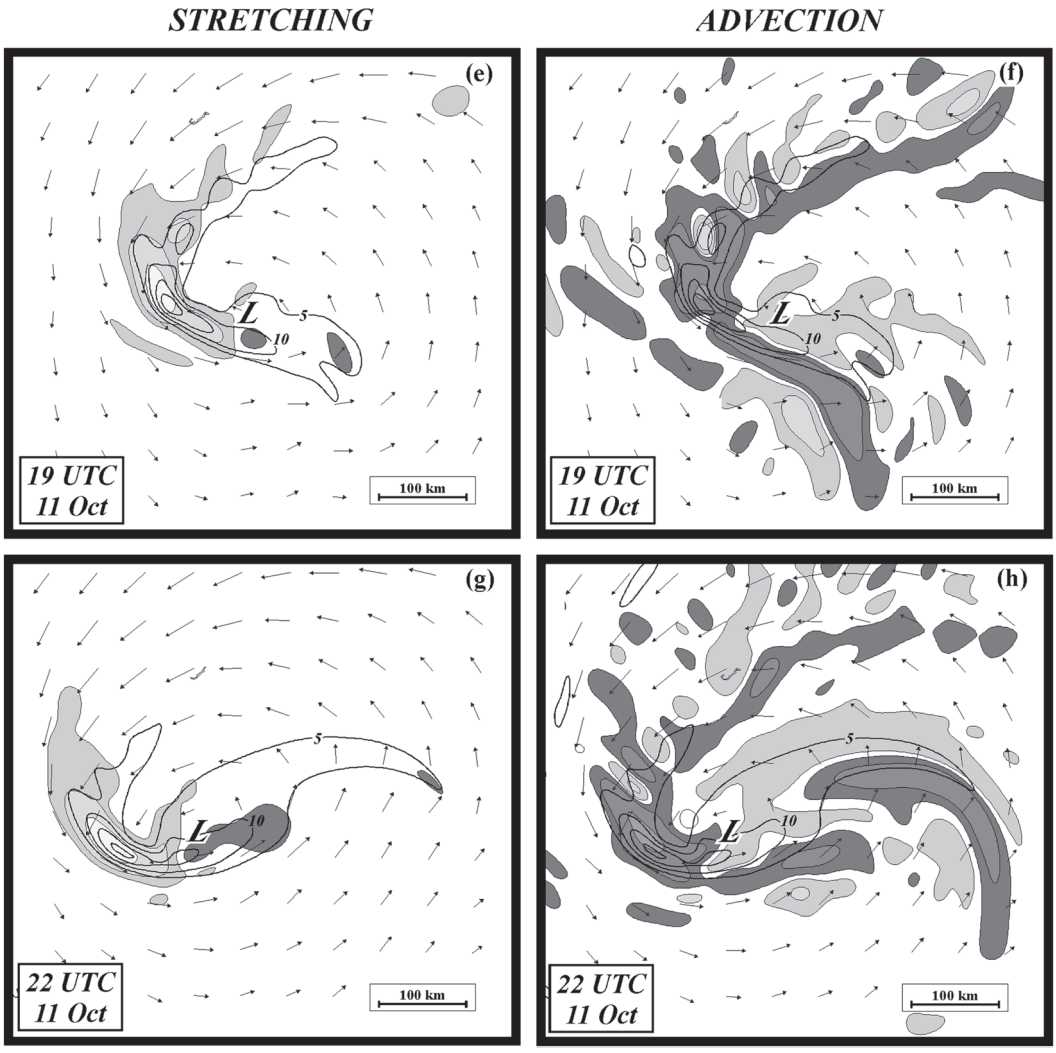

FIG. 10. (*Continued*)

and maximum values of frontogenesis increased sixfold along the bent-back front (Fig. 11c). The cold tongue became even more pronounced and further encircled the western side of the cyclone. On the warm side of the front, low-level PV continued to increase as a consequence of diabatic heating, growing into a robust linear band parallel to the axis of the cold tongue. As low-level absolute and potential vorticity begin to wrap around the SLP minimum, the main band of frontogenesis persisted to the west of the cyclone center and the cold tongue enveloped the southern flank of the storm (Fig. 11d). Eventually the cold tongue fully encircled the transitioning cyclone resulting in the isolation of a warm anomaly near the cyclone center (not shown).

A peculiar feature of the circulation associated with the bent-back front was the development of near-surface negative absolute vorticity, extending along the western and southwestern edge of the cold tongue, in the hours following the initiation of the upshear convection (Fig. 9c). Figures 12–14 show cross sections through the bent-back front prior to and during the outbreak of upshear convection. At 1200 UTC 11 October, a strong updraft occurred at the warm edge of the front while a strong, but rather broad, easterly low-level jet was evident poleward of the front (Fig. 12a). A region of negative absolute vorticity was present just to the northwest of the top of the updraft (Fig. 12b). This updraft transported high θ_e air upward and northwestward over the top of cooler and drier air on the poleward side of the front (Fig. 12c). By 1500 UTC, as the strong upshear convection was developing, an intense, slanted updraft existed with a companion downdraft on the cool, dry side of the front (Fig. 13a). Coincident with the downdraft was an area of negative absolute vorticity that extended into the

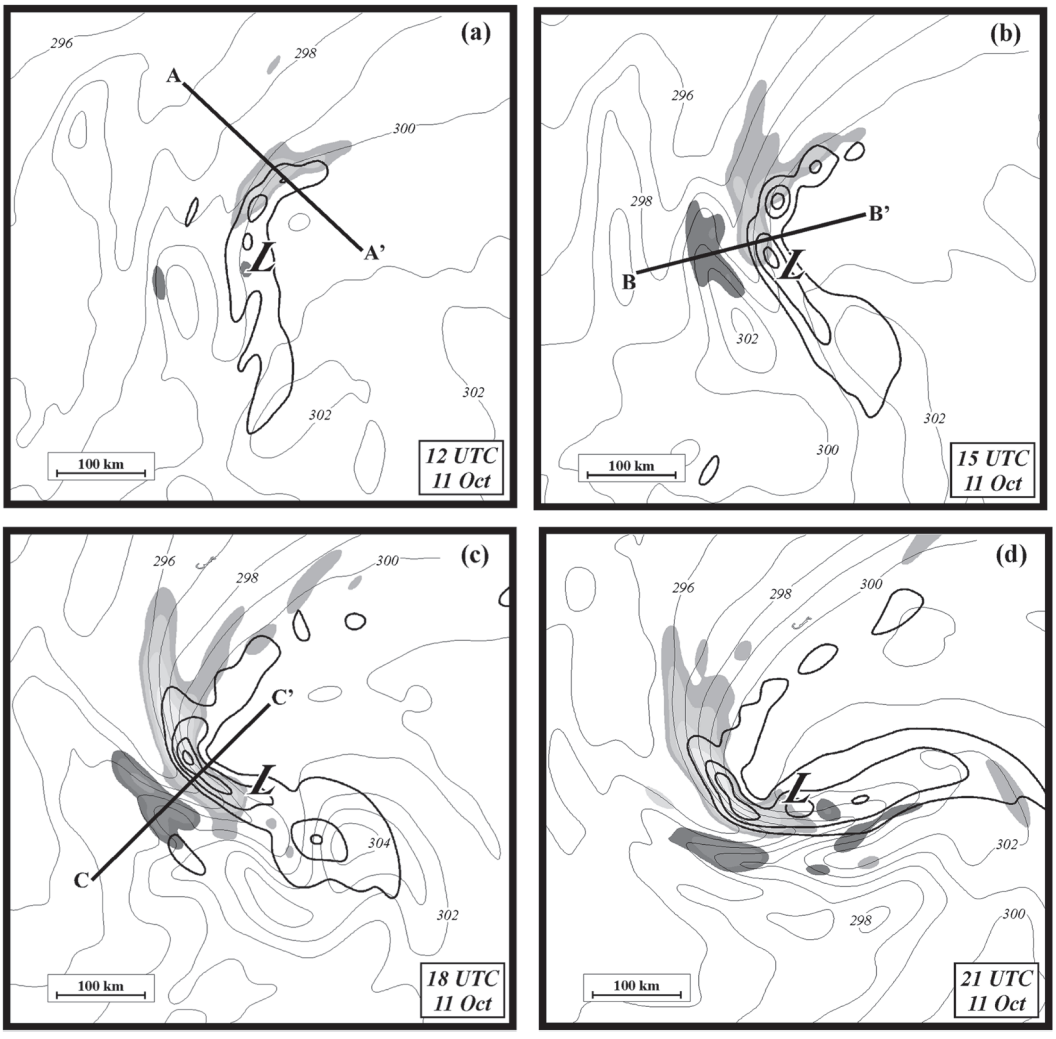

FIG. 11. WRF forecast of 900-hPa potential temperature (thin lines), 850–950-hPa layer PV (thick lines), and 900-hPa frontogenesis (shaded) valid at (a) 1200 UTC 11 Oct 2001, (b) 1500 UTC 11 Oct 2001, (c) 1800 UTC 11 Oct 2001, and (d) 2100 UTC 12 Oct 2001. Potential temperature labeled and contoured as in Fig. 8a. PV contoured every 2 PVU beginning at 2 PVU. Frontogenesis in FGU with positive (negative) values lightly (darkly) shaded in increments of 10, 20, 30, 40, and 80 FGU (−10, −20, −40, and −80 FGU). The "L" in (a)–(d) represents the position of the SLP minimum.

boundary layer (Fig. 13b). Another significant change was the appearance of low-θ_e air on the cold side of the front in the vicinity of the downdraft (Fig. 13c). The situation at 1800 UTC was similar in kind but sharper in degree as the area of negative absolute vorticity became stronger in magnitude, extended closer to the surface, and was coincident with a narrow, intense low-level jet that existed on the cool side of the front adjacent to a tight near-surface θ_e gradient (Figs. 14a–c). Additionally, low-θ_e air continued to intrude toward the surface (Fig. 14c). Thus, there appears to be a relationship between evaporative cooling in the convective downdraft, the downward extension of negative vorticity, the concentration of the LLJ, and the cold tongue.

To identify the source of the air in the cold tongue, trajectories were calculated for parcels in the area of negative absolute vorticity (trajectories were calculated from the model output at hourly intervals using the software package known as VIS5D; more information is available online at http://www.ssec.wisc.edu/~billh/vis5d.html).Figure 15 displays one characteristic trajectory taken backward and forwards from a parcel present in the negative vorticity band at 2100 UTC 11 October at 900 hPa (~1 km). The parcel originated north of the warm front below 850 hPa and initially moved quickly to the west-southwest while slowly ascending in a cold conveyor belt-type flow. By 1700 UTC, the parcel reached the northwest-occluded quadrant of the cyclone

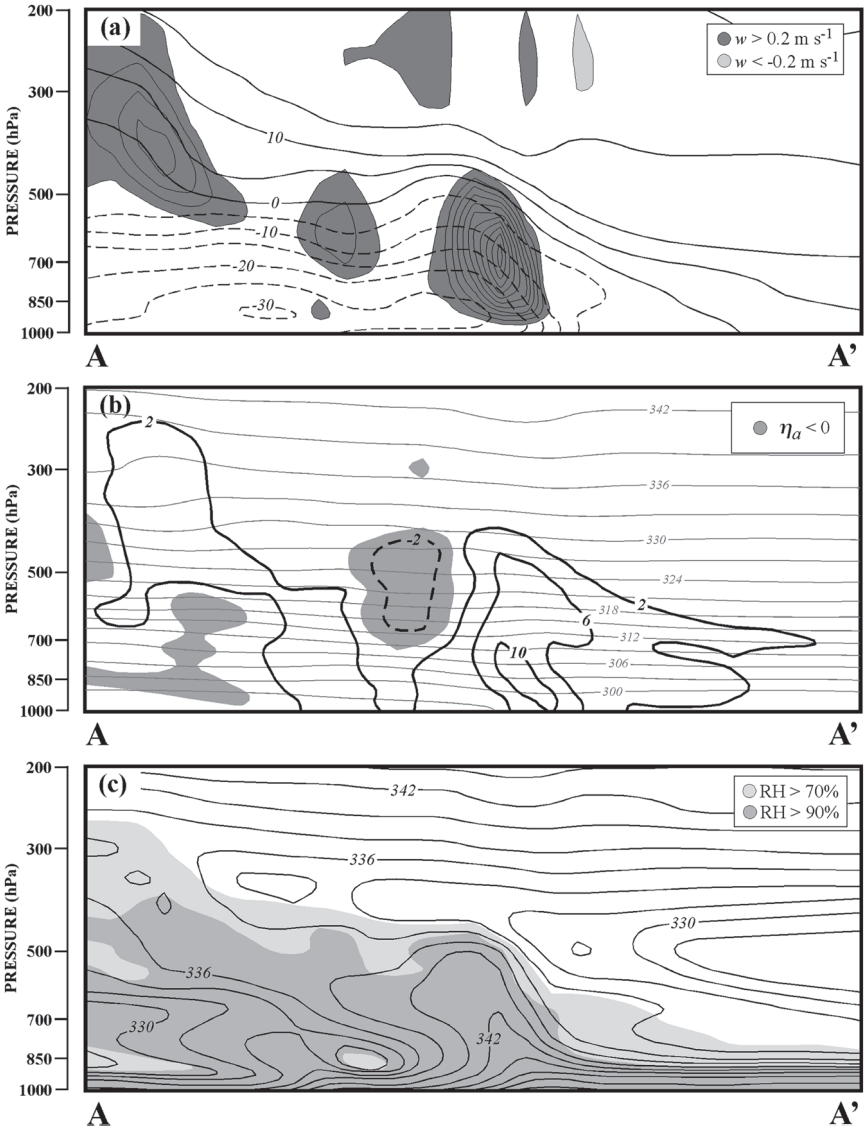

FIG. 12. Cross section along A–A′ in Fig. 10a from the WRF forecast valid at 1200 UTC 11 Oct 2001. (a) Thick lines are contours of wind speed normal to the cross section (m s^{-1}, negative values hatched) and thin lines/shaded areas represent vertical velocity (contoured every 0.2 m s^{-1}, zero contour is excluded). (b) Thick black lines are contours of absolute vorticity (10^{-4} s^{-1}), shaded areas represent areas of negative absolute vorticity, while thin gray lines are isentropes labeled in K and contoured every 3 K. (c) Thick lines are contours of equivalent potential temperature (θ_e, K) and shaded areas represent relative humidity.

and began to rise quickly in an updraft exceeding 0.5 m s^{-1} near the intense upshear convection. During this rapid ascent, as the parcel ascended to its maximum elevation around 600 hPa between 1800 and 1900 UTC, considerable diabatic heating occurred as the parcel's θ increased by 10°C while its mixing ratio decreased by 4.3 g kg^{-1} from 1500 to 1800 UTC. Rapid descent characterized by evaporative cooling followed as the parcel reached the 900-hPa level, having cooled by 16°C with a 5.3 g kg^{-1} increase in mixing ratio, by 2100 UTC. At this time, the parcel was located within the cold tongue and the 30 m s^{-1} LLJ. The relationship between evaporative cooling in the occluded quadrant and the development of this low-level wind speed maximum is reminiscent of the ''sting jet'' described by Browning and colleagues (Browning 2004; Clark et al. 2005). Upon reaching the boundary layer, the parcel began to cyclonically encircle the SLP minimum. Thus, parcels from the cool air north of the warm front were processed by the frontogenesis and upshear convection, evaporatively

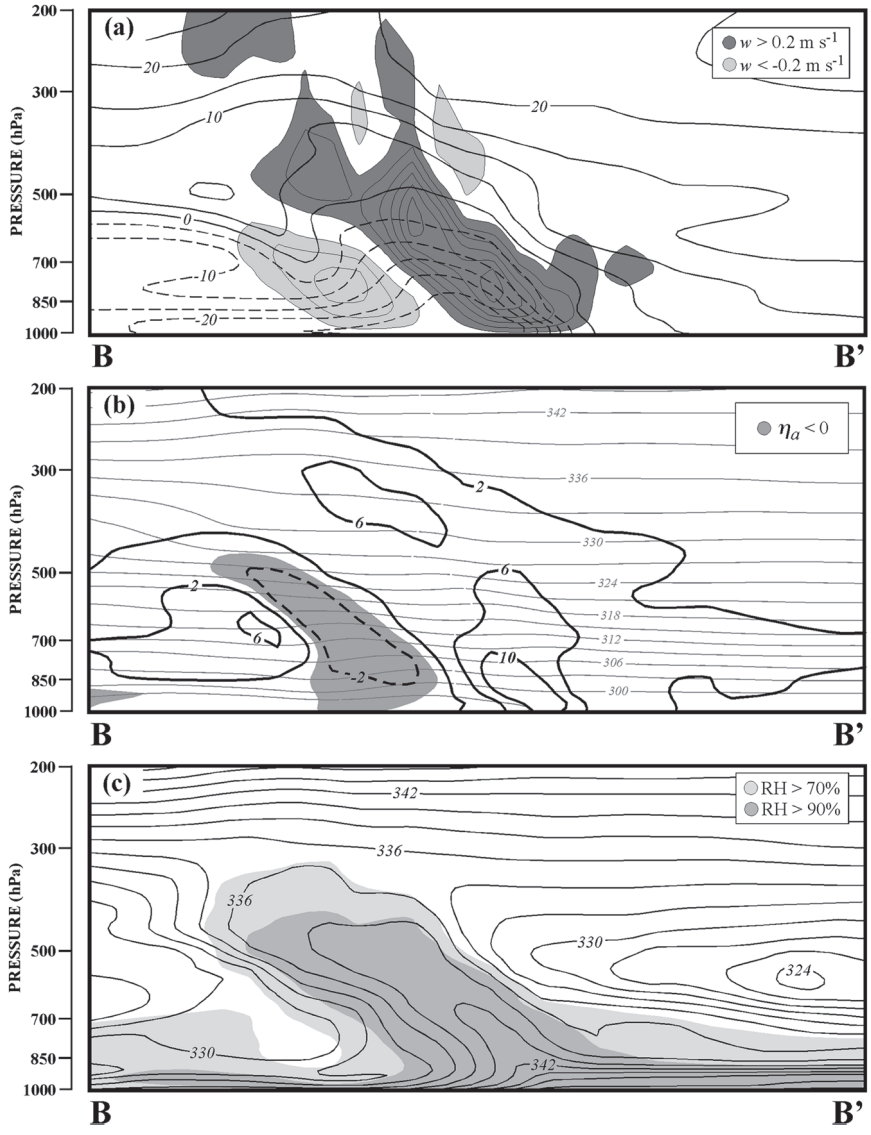

FIG. 13. As in Fig. 12, but along B–B′ in Fig. 10b and from the WRF forecast valid at 1500 UTC 11 Oct 2001.

cooled and then placed into the cold tongue, which rapidly surrounded the cyclone center with cooler air.

d. Potential vorticity

Potential vorticity is conserved for adiabatic, inviscid flow. When diabatic effects are considered the tendency of PV can be represented as

$$\rho \frac{dP}{dt} = \boldsymbol{\eta}_a \cdot \nabla \dot{\theta}, \tag{2}$$

where ρ is the atmospheric density, P is the potential vorticity, $\boldsymbol{\eta}_a$ is the three-dimensional absolute vorticity vector ($\eta_x = \partial v/\partial p$, $\eta_y = -\partial u/\partial p$, η_p), and $\dot{\theta}$ is the diabatic heating rate (Hoskins et al. 1985). From Emanuel et al. (1987), the rate of diabatic heating due to latent heat release H can be estimated as

$$H = \frac{d\theta}{dt} = \omega\left(\frac{\partial\theta}{\partial p} - \frac{\gamma_m}{\gamma_d}\frac{\theta}{\theta_e}\frac{\partial\theta_e}{\partial p}\right), \tag{3}$$

where ω is the vertical motion, θ_e is the equivalent potential temperature, hydrostatic balance is assumed, and γ_d and γ_m are the dry and moist adiabatic lapse rates, respectively. Cammas et al. (1994) used H to find a nonadvective PV flux vector:

$$\mathbf{Y} = -H\boldsymbol{\eta}_a + \nabla_p\theta \times \mathbf{F}, \tag{4}$$

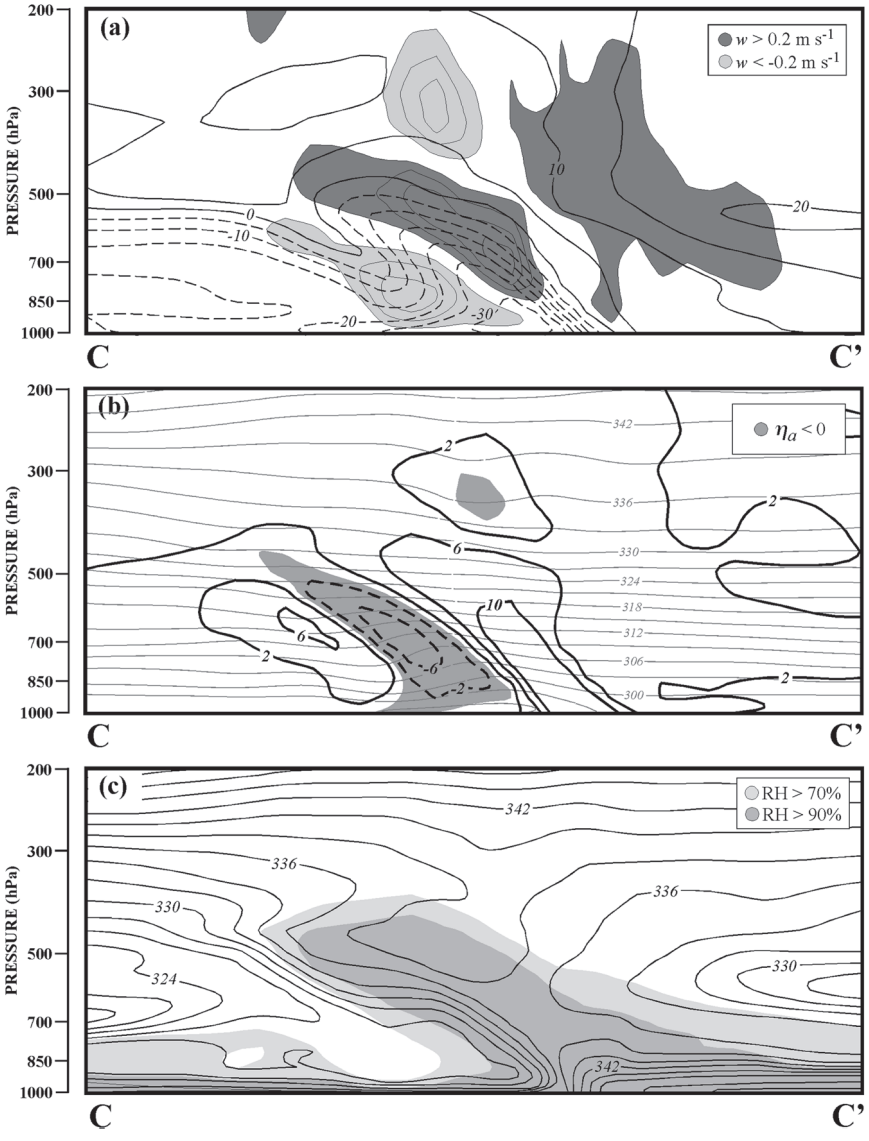

FIG. 14. As in Fig. 12, but along C–C′ in Fig. 10c and from the WRF forecast valid at 1800 UTC 11 Oct 2001.

where ∇_p is the three-dimensional gradient operator $(\partial/\partial x\mathbf{i} + \partial/\partial y\mathbf{j} - \partial/\partial p\mathbf{k})$ and $\mathbf{F}$ is the friction force. Neglecting friction, the nonadvective PV tendency induced by LHR can then be described by

$$\begin{aligned}(\partial P/\partial t)_{\mathrm{LH}} &= -g\nabla_p \cdot \mathbf{Y} \\ &= \boldsymbol{\eta}_a \cdot \nabla_p H \\ &= -\left(\mathbf{k} \times \frac{\partial \mathbf{V}}{\partial p}\right) \cdot \nabla_2 H - \eta \frac{\partial H}{\partial p}, \end{aligned} \tag{5}$$

where ∇_2 is a two-dimensional gradient operator $(\partial/\partial x\mathbf{i} + \partial/\partial y\mathbf{j})$. Thus, given a heating maximum in the midtroposphere and an upward-directed absolute vorticity vector, PV will tend to increase (decrease) below (above) the heating maximum (Raymond 1992). And, when there is a nontrivial amount of vertical shear, the horizontal component of the nonadvective PV tendency [first term on the RHS of (5)] can be large and will increase (decrease) the amount of PV in the direction opposite to (along) the horizontal vorticity vector with a magnitude determined by the product of the magnitudes of the vertical shear and heating rate. Thus, when large vertical shear exists there can be a large horizontal distance between the areas of upper-tropospheric negative PV tendency and near-surface positive PV tendency (Lackmann 2002).

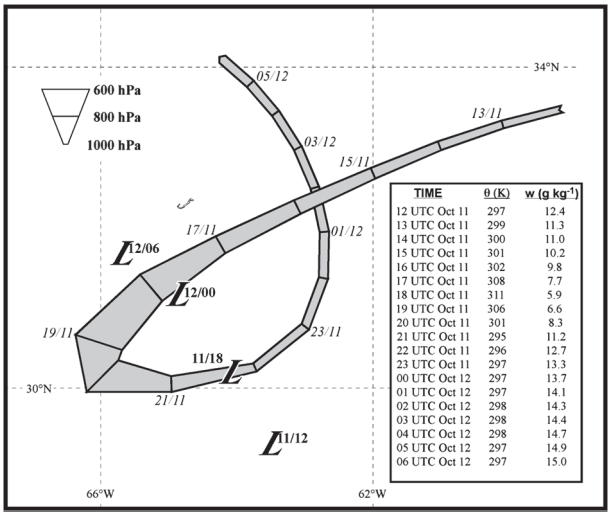

FIG. 15. Absolute trajectory from 1200 UTC 11 Oct 2001 to 0600 UTC 12 Oct 2001 from the WRF model simulation. See text for explanation of significance. Tick marks on each trajectory represent parcel positions along the trajectory at 1-h intervals with times denoted next to the tick marks. The height of the parcel along the trajectory is given by the width scale on the right. The inset lists the parcel's θ and mixing ratio at 1-h intervals along the trajectory path. Each "L" represents the position of the SLP minimum at the denoted time. All times are indicated by the notation time/date.

Figure 16 displays upper- and lower-level PV in isentropic layers along with horizontal vorticity vectors calculated using the 200–900-hPa vertical shear. At the beginning of the simulation, a large upper-level PV maximum existed to the west of the developing cyclone (Fig. 16a). During the first 12 h, there was a slow increase in the low-level PV to the west of the cyclone center along the bent-back warm front (Fig. 16b). Between 1200 and 1800 UTC 11 October, the period of intense upshear convection, near-surface winds increased along the front resulting in a slight increase in vertical shear to the west of the cyclone center. Since shear vectors in this region were mostly southerly, horizontal vorticity vectors were westerly and pointed directly from the maximum of lower PV to the maximum of upper PV. Thus, vertical PV redistribution via LHR was particularly efficient during this period such that, by 1800 UTC 11 October, a large area of the upper PV anomaly had been destroyed and low-level PV to the west of the cyclone had increased (Fig. 16c). Diabatic erosion of the upper-level PV continued through 0000 UTC 12 October while low-level PV continued to increase and amalgamate around the center of the transitioning cyclone (Fig. 16d).

In other studies, upper-level PV destruction (Montgomery and Farrell 1993) and upshear convection (Davis and Bosart 2003, 2004) have been shown to be important precursors to tropical transition. In the present case, the period of intense upshear convection was preceded by an increase in vorticity along the warm front which, in turn, was a by-product of strong low-level frontogenesis there. The resulting increase in near-surface winds also increased the magnitude of vertical shear/horizontal vorticity on the west/upshear side of the cyclone. The juxtaposition of low-level frontogenesis and weak stability west of the cyclone center increased the likelihood of convection. Therefore, the early evolution of the precursor cyclone predisposed convection to occur on the upshear side in an area where PV redistribution was particularly efficient.

Posselt and Martin (2004) found that during the extratropical occlusion process diabatic heating via LHR erodes upper-level PV and eventually forms a notch (a local negative PV anomaly) in the upper-level PV field. The formation of this notch serves to isolate the positive PV anomaly from the midlatitude flow and imposes a circulation that encourages negative PV advection into the notch. This process results in the acquisition of the treble clef PV structure. To assess the similarity between this view of the extratropical occlusion process and the simulated tropical transition of Karen, we perform a similar analysis calculating diabatic heating rates from (3) and nonadvective PV tendencies from (5). Maximum values for the heating rates and PV tendencies are 25 K h^{-1} and -5.0 PVU h^{-1} (1 PVU $\equiv 10^{-6}$ m^2 s^{-1} K kg^{-1}), respectively, which are much higher than rates calculated by Posselt and Martin (2004),[3] evidence that the convection in Karen was much stronger than that found in association with typical high-latitude, cool season extratropical cyclones.

Figure 17 displays both the diabatically generated and advective PV tendencies on an isentropic surface near the tropopause around the time of the burst of upshear convection. At 1200 UTC 11 October, the upper-level PV feature had large magnitude and areal distribution. Negative diabatic PV tendency was far to the east of the anomaly in association with convection along the cyclone's warm front (Fig. 17a) while negative PV advection was generally of small magnitude and disorganized (Fig. 17b). By 1800 UTC during the outbreak of upshear convection, an intense area of nonadvective, negative PV tendency existed to the west of the cyclone and contributed to the formation of the notch in the treble clef structure (Fig. 17c). As a result of ridge building downstream of the convection, upper-level winds west

[3] Posselt and Martin (2004) used the same formulation to calculate both diabatic heating rates and PV destruction rates.

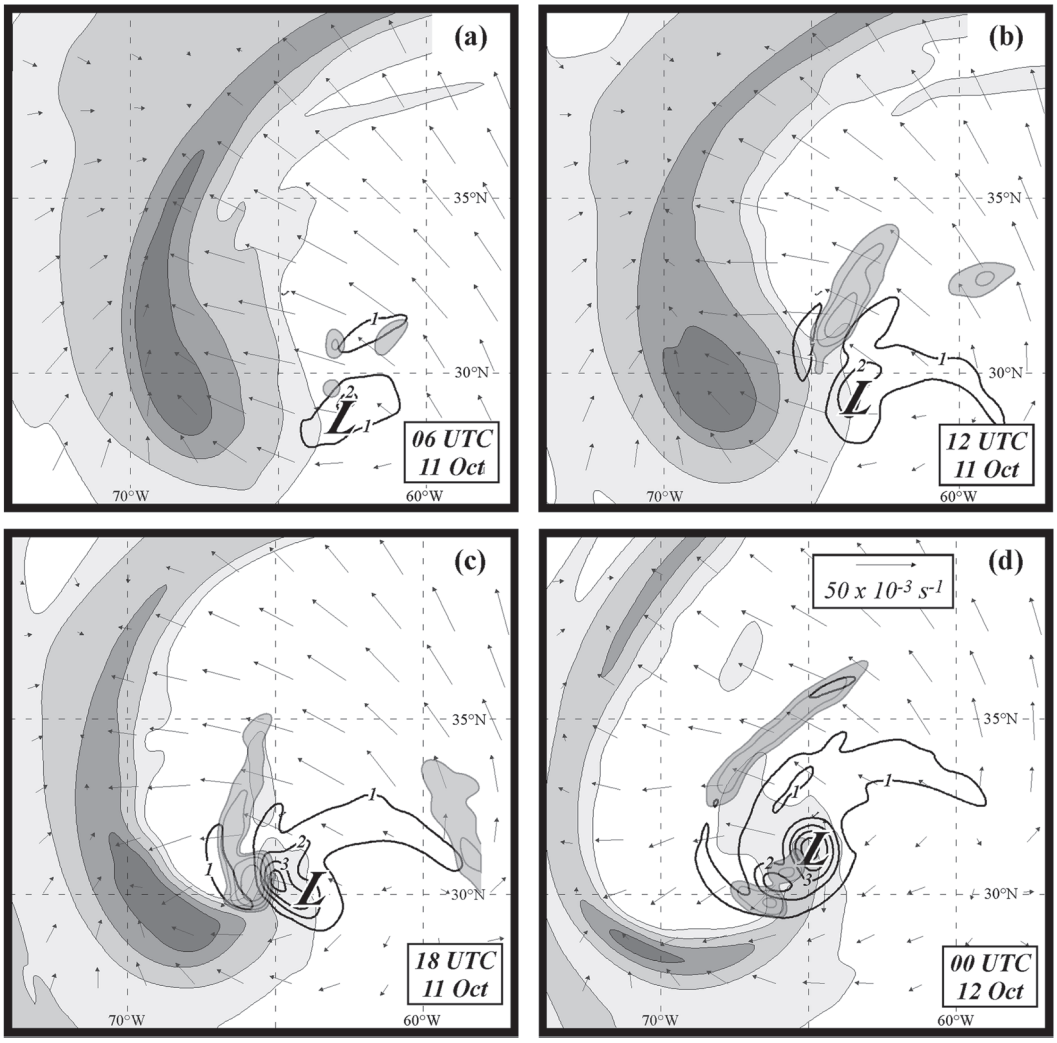

FIG. 16. WRF forecast of 305–315-K PV (thick lines), 335–345-K PV (shaded), horizontal vorticity vectors (derived from 200–900-hPa vertical shear), and 340-K PV dilution (light shading) valid at (a) 0600 UTC 11 Oct 2001, (b) 1200 UTC 11 Oct 2001, (c) 1800 UTC 11 Oct 2001, and (d) 0000 UTC 12 Oct 2001. 305–315-K PV is in PVU and contoured every 1 PVU beginning at 1 PVU. 335–345-K PV is shaded in increments of 1, 2, 4, and 6 PVU. PV dilution in units of PVU day^{-1} and shaded at intervals of −2, −4, −8, and −16 PVU day^{-1}. The "L" in (a)–(d) represents the position of the SLP minimum.

of the center turned counterclockwise over time and become more parallel to the strong PV gradient. Hence, a large area of negative PV advection, with magnitudes similar to those of the diabatic tendency, occurred to the west and southwest of the cyclone at this time (Fig. 17d). Six hours later (0000 UTC 12 October), the diabatic tendency had lessened but rotated counterclockwise to the south of the SLP minimum (Fig. 17e). Significant negative PV advection was still occurring, however, and the strong PV gradient continued to be pushed to the south away from the cyclone (Fig. 17f).

Thus, the upshear convection initiated a process that resulted in destruction of PV via LHR and introduced a component to the upper-level winds, which moved the upper-level PV anomaly, and strong PV gradient, away from the transitioning cyclone. Consequently, vertical shear over the transitioning cyclone decreased to below 15 m s^{-1} by 0600 UTC 12 October (Table 1), facilitating the acquisition of tropical characteristics. This entire process is similar to that described by Posselt and Martin (2004) except that in the present case the amplitude of the upper-level PV anomaly is initially smaller and the intensity of the convection is much greater, a combination that results in the almost total annihilation of the upper-level PV feature.

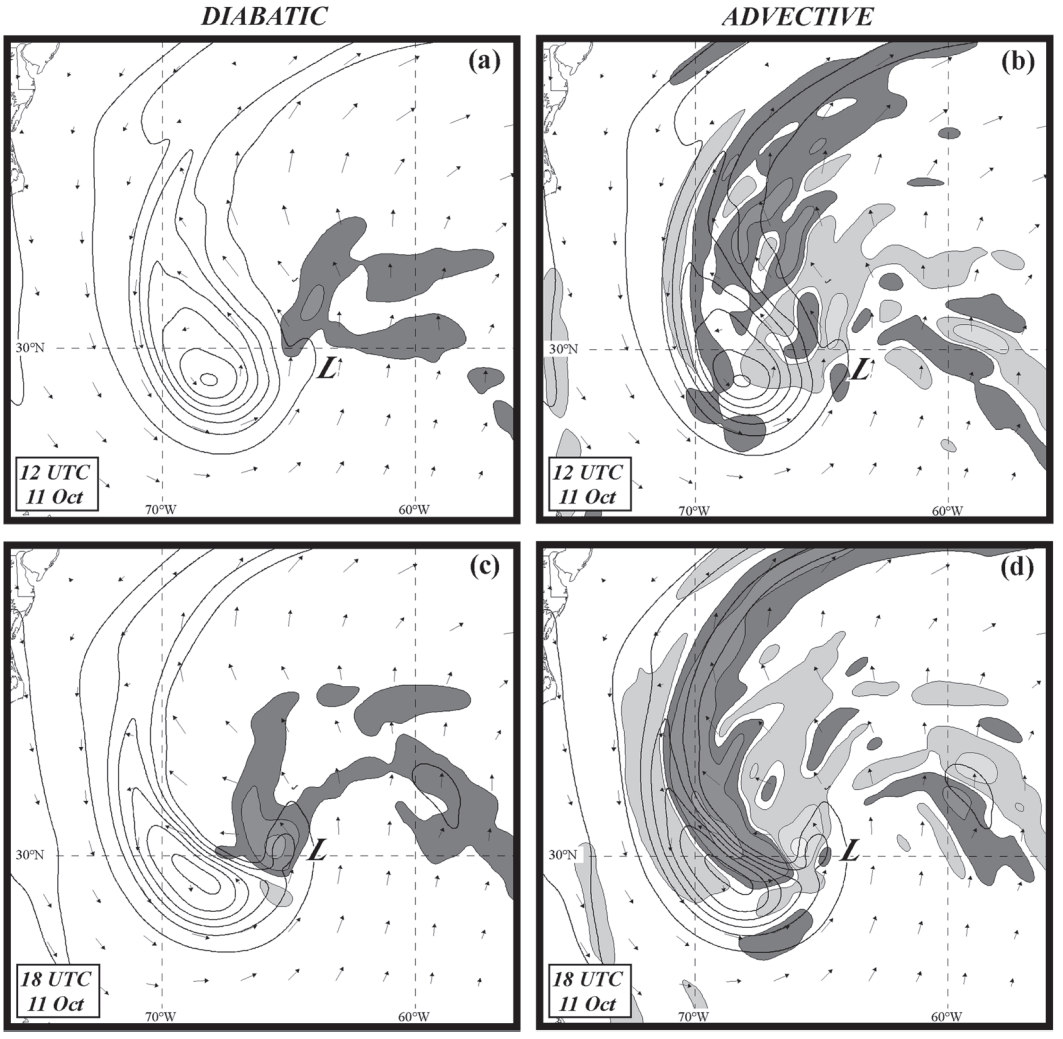

FIG. 17. (a) Diabatically generated (nonadvective) PV tendency in the 330–340-K layer (shaded), 330–340-K layer PV, and 335-K wind vectors from the WRF forecast valid at 1200 UTC 11 Oct 2001. PV tendency is in units of PVU h^{-1} with positive (negative) values lightly (darkly) shaded in increments of 0.1, 0.5, and 2 PVU h^{-1} (-0.1, -0.5, and -2 PVU h^{-1}). (b) Advective PV tendency in the 330–340-K layer (shaded) and 330–340-K layer PV from the WRF forecast valid at 1200 UTC 11 Oct 2001. Variables contoured and shaded as in (a). (c) As in (a), but from the WRF forecast valid at 1800 UTC 11 Oct 2001. (d) As in (b), but from the WRF forecast valid at 1800 UTC 11 Oct 2001. (e) As in (a), but from the WRF forecast valid at 0000 UTC 12 Oct 2001. (f) As for (b), but from the WRF forecast valid at 0000 UTC 12 Oct 2001. The ''L'' in (a)–(f) represents the position of the SLP minimum.

5. Summary and discussion

Prior work on tropical transition has outlined a set of physical processes that can transform a strongly sheared, cold-core, baroclinic storm into a weakly sheared, axisymmetric, warm-core tropical cyclone. The present analysis supports the findings of Davis and Bosart (2003) that the precursor to transition develops like an ordinary extratropical cyclone as an upper-tropospheric trough encroaches upon a low-level baroclinic zone inducing upward vertical motion via cyclonic vorticity advection by the thermal wind (Sutcliffe 1947) and distorting the linear baroclinic zone into a frontal wave (Martin 2006). Eventually, a closed circulation and sea level pressure minimum form at the surface. The extratropical precursor progresses through a life cycle similar to that described by Shapiro and Keyser (1990) with a bent-back warm/occluded front extending into the cool air west and northwest of the surface cyclone center. Davis and Bosart (2004) suggest that the presence of a bent-back

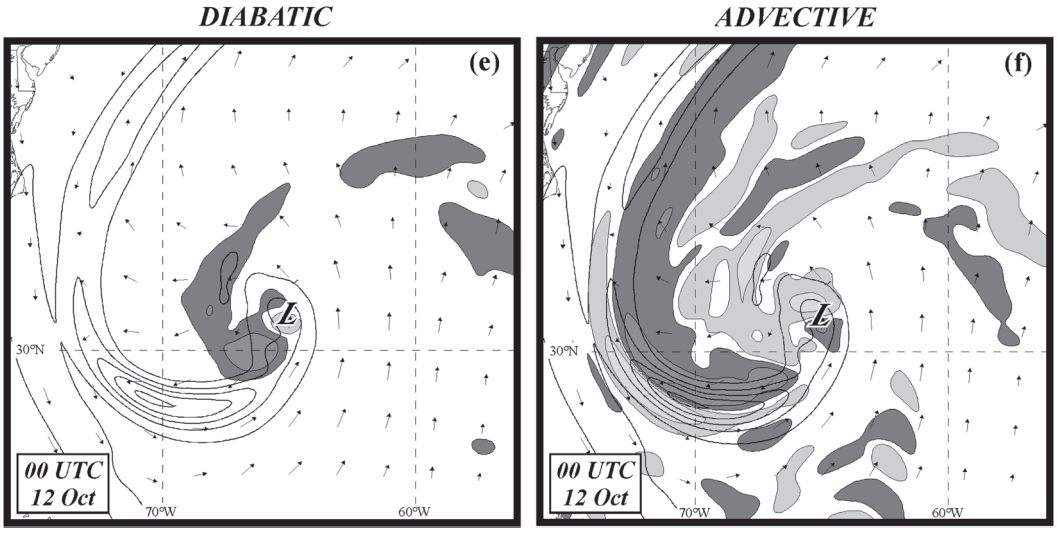

FIG. 17. (*Continued*)

front may be important to the extent that it testifies to a stronger precursor storm from which it is easier to transition. In addition, they acknowledge the ubiquity of upshear convection along this front in the transition of SECs (an observation supported by the analysis of Part I). In their model-aided analysis of Hurricane Michael, Davis and Bosart (2003) considered the manner by which convection was organized by circulations characteristic of the extratropical cyclone life cycle.

The present analysis has identified an area of frontogenesis that develops coincident with this front and becomes more intense with time. Within the resultant circulation, precipitation forms and promotes low-level, diabatic PV generation through latent heat release. The increase in PV leads to further strengthening of the low-level winds north of the warm front. Since these low-level winds are either northeasterly or northerly and tropopause-level winds downstream of the upper trough are southerly or southwesterly, vertical shear over the western half of the cyclone increases to greater than 50 m s^{-1}. The combination of frontogenesis and weak stability in the occluded quadrant preconditions the western semicircle of the cyclone for deep convection.

In such an environment, an intense burst of convection eventually occurs on the upshear side of the cyclone. This convection initiates three processes that are essential to the tropical transition of the cyclone. The first process concerns the amalgamation of low-level vorticity and intensification of the circulation about the cyclone center. The upshear convection produces a large-amplitude vorticity maximum along the bent-back front resulting in an asymmetric vorticity field with the stronger vorticity in the cyclone's western half becoming the dominant feature in the cyclone. Also in association with the convection, downdraft generation via evaporative cooling leads to the development of an intense northwesterly low-level jet that is directed slightly across the front. By means of positive vorticity advection, this cross-front flow contributes to an accumulation of vorticity at a reforming cyclone center. Though the process by which additional consolidation of this isolated vorticity maximum occurs is a topic for further study, the observed westward jog of the precursor, a characteristic of each of the cases examined in Part I, is likely a response to the formation of a smaller-scale vortex tied to column stretching associated with the upshear convection. Such a suggestion has been made in other studies (e.g., Molinari et al. 2004) of moderately sheared tropical cyclogenesis.

Second, the upshear convection accelerates the advection of cooler, drier air around the cyclone center through intensifying the circulation around the cyclone and dumping evaporatively cooled air into the boundary layer via convective downdrafts, a process observed to occur in marine cyclones (Kuo et al. 1992). In tropical transition, the air parcel trajectories and frontal structures characterizing this process are similar to those associated with maritime extratropical storms but are more intensely influenced by the convection. Specifically, parcels of air that originate north of the cyclone's warm front ascend as they head to the southwest poleward of the warm front until they are sent to the surface by the downdraft associated with the upshear convection. That downdraft places evaporatively cooled air on the already cold side of the front, increasing the temperature contrast and intensifying the frontogenesis.

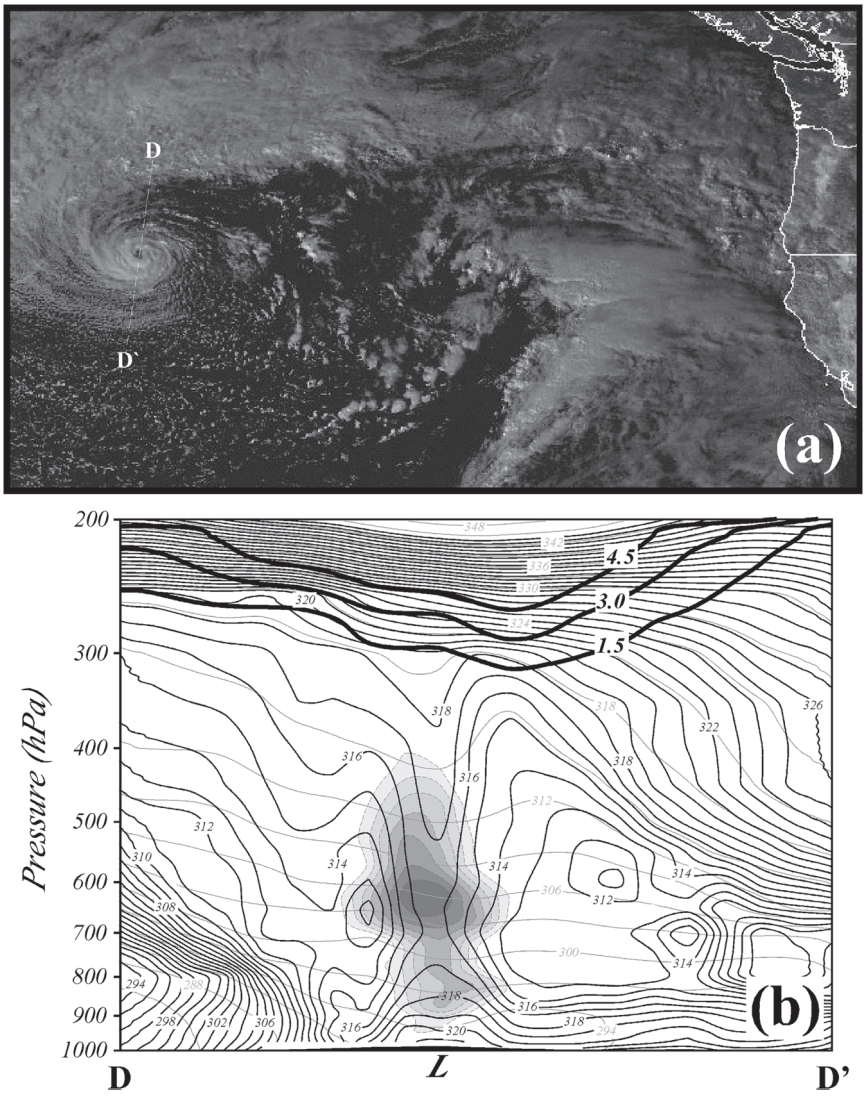

FIG. 18. (a) *GOES-10* visible satellite image from 0045 UTC 2 Nov 2006 showing the unnamed Pacific storm about 1100 km off the coast of Oregon. (b) Vertical cross section along line D–D' is shown. Sea surface temperatures beneath the storm were ~16°C. (b) Vertical cross section along line D–D' in (a) of θ_e, θ and PV from the 0000 UTC 2 Nov 2006 FNL analysis. The quantity θ_e is labeled in K and contoured every 1 K. Tropospheric PV is shaded in increments of 0.1 PVU beginning at 0.7 PVU. Thick black lines are upper-tropospheric/lower-stratospheric PV labeled in PVU and contoured every 1.5 PVU beginning at 1.5 PVU. Thin gray lines are θ_v isentropes labeled in K and contoured every 3 K. "L" represents the position of the SLP minimum along the cross section.

The resultant frontogenetic circulation, and its diabatically generated low-level PV, intensifies the low-level jet, which then advects the cool air around the western and southern quadrants of the cyclone center.

Last, upshear convection is principally responsible for redistributing PV in the vertical (via latent heat release) and altering the upper-level environment above the cyclone so as to reduce the vertical shear and accommodate the sustenance of a fully tropical cyclone. Early in the life cycle when precipitation is mostly downshear of the cyclone, alteration of the PV field is limited to upper-level ridging to the north and east of the PV anomaly. While this ridging serves to isolate the upper-level PV anomaly from the midlatitude westerlies, the initial convection has no effect on changing the environment in the immediate vicinity of the cyclone. The analysis suggests that the alterations to the PV field surrounding the cyclone that are necessary to instigate

transition cannot occur until convection develops upshear/west of the storm. Given the westward-pointing horizontal vorticity vector described earlier, upshear convection is particularly efficient at transferring high PV from the upper-level trough to the surface cyclone, a suggestion made by Davis and Bosart (2004, see their Fig. 3). This process simultaneously reduces the magnitude of the vertical shear above the cyclone while creating a strong low-level PV anomaly resulting in the creation of a vortex with tropical storm–force winds and a warm core, with little or no baroclinicity, in an environment of weak vertical shear (i.e., the canonical tropical cyclone environment).

Davis and Bosart (2004) suggest that the path to occlusion in transition events is driven by diabatic heating. This is consistent with an emerging view of the extratropical occlusion process, suggested by the analysis of Posselt and Martin (2004), in which latent heat release is an essential component. This more comprehensive view of occlusion, with its incorporation of diabatic effects, further underscores the importance of occlusion of the precursor disturbance in tropical transition.

Other studies of tropical transition (Bosart and Bartlo 1991; Montgomery and Farrell 1993; Davis and Bosart 2001, 2003, 2004) have stressed the importance of upshear convection in transforming the synoptic environment into one favorable for tropical cyclones by substantially weakening the upper-level trough/cold dome. While a similar observation is made here, we advance the theory that upshear convection is a strongly forced, important component of a comprehensive transition process involving frontal dynamics and latent heat release and not a random event whose occurrence triggers the transition of otherwise suitably preconditioned storms. In fact, upshear convection acts as a bridge between extratropical and tropical dynamics; expediting the extratropical occlusion process on the one hand while simultaneously initiating the tropical cyclogenesis process on the other.

The study of the tropical transition of strong extratropical precursors suggests that a continuum of dynamical processes and developmental mechanisms link extratropical and tropical cyclogenesis. It is well known, for instance, that the intensity of many maritime cyclones is enhanced through storm-induced fluxes of latent and sensible heat (e.g., Uccellini 1990; Reed et al. 1991) not generally available to continental storms. Davis and Bosart (2003) suggest that the equilibration (i.e., occlusion) of maritime baroclinic cyclones tends to produce an environment conducive to tropical cyclogenesis. This is a result of the fact that occlusion, by virtue of its dependence on latent heating, involves considerable diabatic rearrangement of PV and an attendant alteration in the vertical shear above the cyclone center. Recent intriguing cases of apparent tropical transition such as Catarina off the coast of Brazil in March 2004 (Pezza and Simmonds 2005; McTaggart-Cowan et al. 2006) or an unnamed storm over the northeast Pacific Ocean in November 2006 (Fig. 18) have developed over waters as much as 10°C colder than the accepted threshold for tropical cyclogenesis. Such cases would appear to be ideal candidates for further study of the relative roles of extratropical postmature phase dynamics versus air–sea interaction in the tropical transition process.

Acknowledgments. This work was supported by grants from the National Science Foundation (NSF-0202012 and NSF-0452318). Discussions with Drs. Michael Morgan and Gregory Tripoli are greatly appreciated. The careful reviews of Drs. Chris Davis and Ron McTaggart-Cowan are also gratefully acknowledged.

REFERENCES

Bancroft, G. P., 2002: Marine weather review: North Atlantic area September through December 2001. *Mar. Wea. Log,* **46,** 1–13.

Beven, J. L., S. R. Stewart, M. B. Lawrence, L. A. Avila, J. L. Franklin, and R. J. Pasch, 2003: Atlantic hurricane season of 2001. *Mon. Wea. Rev.,* **131,** 1454–1484.

Bosart, L. F., and J. A. Bartlo, 1991: Tropical storm formation in a baroclinic environment. *Mon. Wea. Rev.,* **119,** 1979–2013.

Browning, K. A., 2004: The sting at the end of the tail: Damaging winds associated with extratropical cyclones. *Quart. J. Roy. Meteor. Soc.,* **130,** 375–399.

Cammas, J.-P., D. Keyser, G. M. Lackmann, and J. Molinari, 1994: Diabatic redistribution of potential vorticity accompanying the development of an outflow jet within a strong extratropical cyclone. Preprints, *Int. Symp. on the Life Cycles of Extratropical Cyclones,* Vol. II, Bergen, Norway, Geophysical Institute, University of Bergen, 403–409.

Clark, P. A., K. A. Browning, and C. Wang, 2005: The sting at the end of the tail: Model diagnostics of fine-scale three-dimensional structure of the cloud head. *Quart. J. Roy. Meteor. Soc.,* **131,** 2263–2292.

Davis, C. A., and K. A. Emanuel, 1991: Potential vorticity diagnostics of cyclogenesis. *Mon. Wea. Rev.,* **119,** 1929–1953.

——, and L. F. Bosart, 2001: Numerical simulations of the genesis of Hurricane Diana (1984). Part I: Control simulation. *Mon. Wea. Rev.,* **129,** 1859–1881.

——, and ——, 2003: Baroclinically induced tropical cyclogenesis. *Mon. Wea. Rev.,* **131,** 2730–2747.

——, and ——, 2004: The TT problem: Forecasting the tropical transition of cyclones. *Bull. Amer. Meteor. Soc.,* **85,** 1657–1662.

Dudhia, J., 1989: Numerical study of convection observed during the winter monsoon experiment using a mesoscale two-dimensional model. *J. Atmos. Sci.,* **46,** 3077–3107.

Emanuel, K. A., M. Fantini, and A. J. Thorpe, 1987: Baroclinic instability in an environment of small stability to slantwise moist convection. Part I: Two-dimensional models. *J. Atmos. Sci.,* **44,** 1559–1573.

Hart, R. E., 2003: A cyclone phase space derived from thermal wind and thermal asymmetry. *Mon. Wea. Rev.,* **131,** 585–616.

Hong, S.-Y., and J.-O. J. Lim, 2006: The WRF single-moment microphysics scheme (WSM6). *J. Korean Meteor. Soc.,* **42,** 129–151.

——, Y. Hoh, and J. Dudhia, 2006: A new vertical diffusion package with an explicit treatment of entrainment processes. *Mon. Wea. Rev.,* **134,** 2318–2341.

Hoskins, B. J., M. E. McIntyre, and A. W. Robertson, 1985: On the use and significance of isentropic potential vorticity maps. *Quart. J. Roy. Meteor. Soc.,* **111,** 877–946.

Hulme, A. L., and J. E. Martin, 2009: Synoptic- and frontal-scale influences on tropical transition events in the Atlantic basin. Part I: A six case survey. *Mon. Wea. Rev.,* **137,** 3605–3625.

Jones, S. C., and Coauthors, 2003: The extratropical transition of tropical cyclones: Forecast challenges, current understanding, and future directions. *Wea. Forecasting,* **18,** 1052–1092.

Kain, J. S., and J. M. Fritsch, 1990: A one-dimensional entraining/detraining plume model and its application in convective parameterization. *J. Atmos. Sci.,* **47,** 2784–2802.

——, and ——, 1993: Convective parameterization for mesoscale models: The Kain–Fritcsh scheme. *The Representation of Cumulus Convection in Numerical Models,* K. A. Emanuel and D. J. Raymond, Eds., Amer. Meteor. Soc., 165–170.

Korner, S. O., and J. E. Martin, 2000: Piecewise frontogenesis from a potential vorticity perspective: Methodology and a case study. *Mon. Wea. Rev.,* **128,** 1266–1288.

Kuo, Y.-H., R. J. Reed, and S. Low-Nam, 1992: Thermal structure and airflow in a model simulation of an occluded marine cyclone. *Mon. Wea. Rev.,* **120,** 2280–2297.

Lackmann, G. M., 2002: Cold-frontal potential vorticity maxima, the low-level jet, and moisture transport in extratropical cyclones. *Mon. Wea. Rev.,* **130,** 59–74.

Martin, J. E., 1998: The structure and evolution of a continental winter cyclone. Part I: Frontal structure and the classical occlusion process. *Mon. Wea. Rev.,* **126,** 303–328.

——, 2006: The role of shearwise and transverse quasi-geostrophic vertical motions in the mid-latitude cyclone life cycle. *Mon. Wea. Rev.,* **134,** 1174–1193.

McTaggart-Cowan, R., L. F. Bosart, C. A. Davis, E. H. Atallah, J. R. Gyakum, and K. A. Emanuel, 2006: Analysis of Hurricane Catarina (2004). *Mon. Wea. Rev.,* **134,** 3029–3053.

Mlawer, E. J., S. J. Taubman, P. D. Brown, M. J. Iacono, and S. A. Clough, 1997: Radiative transfer for inhomogeneous atmosphere: RRTM, a validated correlated-k model for the long-wave. *J. Geophys. Res.,* **102,** 16 663–16 682.

Molinari, J., D. Vollaro, and K. L. Corbosiero, 2004: Tropical cyclone formation in a sheared environment: A case study. *J. Atmos. Sci.,* **61,** 2493–2509.

Montgomery, M. T., and B. F. Farrell, 1993: Tropical cyclone formation. *J. Atmos. Sci.,* **50,** 285–310.

Pezza, A. B., and I. Simmonds, 2005: The first South Atlantic hurricane: Unprecedented blocking, low shear and climate change. *Geophys. Res. Lett.,* **32,** L15712, doi:10.1029/2005GL023390.

Posselt, D. J., and J. E. Martin, 2004: The effect of latent heat release on the evolution of a warm occluded thermal structure. *Mon. Wea. Rev.,* **132,** 578–599.

Raymond, D. J., 1992: Nonlinear balance and potential vorticity thinking at large Rossby number. *Quart. J. Roy. Meteor. Soc.,* **118,** 987–1015.

Reed, R. J., Y. H. Kuo, and S. Low-Nam, 1991: Effects of surface energy during the early development and rapid intensification stages of seven explosive cyclones in the western Atlantic. *Mon. Wea. Rev.,* **119,** 457–476.

Shapiro, M. A., and D. Keyser, 1990: Fronts, jets streams, and the tropopause. *Extratropical Cyclones: The Erik Palmén Memorial Volume,* C. W. Newton and E. Holopainen, Eds., Amer. Meteor. Soc., 167–191.

Skamarock, W. C., J. B. Klemp, J. Dudhia, D. O. Gill, D. M. Barker, W. Wang, and J. G. Powers, 2005: A description of the advanced research WRF version 2. NCAR Tech. Note NCAR/TN-468+STR, 88 pp.

Sutcliffe, R. C., 1947: A contribution to the problem of development. *Quart. J. Roy. Meteor. Soc.,* **73,** 370–383.

Uccellini, L. W., 1990: Processes contributing to the rapid development of extratropical cyclones. *Extratropical Cyclones: The Erik Palmen Memorial Volume,* C. W. Newton and E. O. Holopainen, Eds., Amer. Meteor. Soc., 81–105.